Computational Study of the Effect of Mineral Dust on Secondary Organic Aerosol Formation by Accretion Reactions of Closed-Shell Organic Compounds

Fatemeh Keshavarz*[,a], Anna Shcherbacheva[a], Jakub Kubečka[a], Hanna Vehkamäki[a], Theo Kurtén[b]

a) Institute for Atmospheric and Earth System Research, Faculty of Science, University of Helsinki, FI-00014, Finland
b) Department of Chemistry, Faculty of Science, University of Helsinki, FI-00014, Finland

* Corresponding author: Fatemeh Keshavarz: fatemeh.keshavarz@helsinki.fi

ABSTRACT

The effect of dust aerosols on accretion reactions of water, formaldehyde and formic acid was studied in the conditions of Earth's troposphere using at the DLPNO-CCSD(T)/aug-cc-pVTZ//ωB97X-D/6-31++G** level of theory. Detailed analysis of the reaction mechanisms in the gas phase and on the surface of mineral dust, represented by mono- and tri-silicic acid, revealed that mineral dust has the potential for decreasing reaction barrier heights. Specifically, at 0 K, mineral dust can lower the apparent energy barrier of the reaction of formaldehyde with formic acid to zero. However, when the entropic contributions to the reaction free energies were accounted for, mineral dust was found to selectively enhance the reaction of water with formaldehyde, while inhibiting the reaction of formaldehyde and formic acid, in the lower parts of the troposphere (with temperatures around 298 K). In the upper troposphere (with temperatures closer to 198 K), mineral dust catalyzes both reactions, and also the reaction of methanol with formic acid. Despite the intrinsic potential of mineral dust, calculation of the catalytic enhancement parameter for a likely range of dust aerosol concentrations suggested that dust aerosols will not contribute to secondary organic aerosol formation via dimerization of closed-shell organic compounds. The main reason for this is the relatively low absolute concentration of tropospheric dust aerosol, and its inefficiency in increasing the effective reaction rate coefficients.

1. INTRODUCTION

Aerosols affect the climate and the quality of human life in many ways. Their impacts include visibility reduction[1], regulation of precipitation by acting as cloud condensation nuclei[2], altering biogeochemical cycles[3], controlling the energy budget of Earth through radiative forcing[3] and imposing adverse health effects[4,5].[6] While the contribution of mineral dust to atmospheric aerosols is noticeable, and mineral dust is emitted to the atmosphere at a high rate, organic materials usually dominate fine atmospheric aerosols[5,7,8]. To be more specific, the total global emission rates of mineral dust particles with the 0.1-1.0 μm and 0.1-10.0 μm particle sizes are estimated to be 48 and 10100 Tg yr^{-1}, respectively. In comparison, the global emissions of organic aerosols are about 200 Tg yr^{-1}.[9] Moreover, around 20 to 60% of the total mass of atmospheric aerosols observed in the continental mid-latitudes, and up to 90% in tropical forested areas, have been found to consist of organic materials[1]. Organic aerosols can be divided into primary organic aerosols (POAs; the organic matter. emitted directly from natural and anthropogenic sources) and secondary organic aerosols (SOAs; the organic matter emitted in gaseous form and transformed to particles in the atmosphere via different reaction paths whether forming entirely new particles or condensing on pre-existing particles[10])[1,7,11]. The amount of SOAs exceeds that of POAs even in heavily urbanized areas[11] and SOAs can form up to 90% of the total organic mass of atmospheric aerosols.[5,12]

Though SOAs and POAs are abundant and display profound impacts on the Earth's climate, their composition has been poorly understood since their chemistry is highly complex[13] and variable with life time,[14] and experimental measurements are bound to large uncertainties[15] due to the difficulty of detecting low volatility compounds with high molecular weights[16].[1] Regardless the complex chemistry, two general routes have been suggested for SOA formation. The first route is related to gas-phase oxidation of volatile organic compounds by ozone, hydroxyl radical (OH), nitrate radical (NO_3) and other atmospheric oxidants, which leads to both fragmentation (ultimately to CO_2), and also production of organic compounds with multiple functional groups. The polyfunctional products with intermediate or low volatilities may then partition onto pre-existing organic aerosols, increasing the SOA mass.[17] The second route occurs in the particle phase. In this route, the gas- and liquid-phase atmospheric oxidants oxidize the organic compounds of aerosols, also leading to an increase in the organic mass[18]. This process is one of the processes involved in aerosol aging[19]. In addition, in the second route, non-oxidative combination of organic compounds can generate high molecular weight oligomers[20,21]. Such accretion reactions[22] have attracted much interest since they can produce organic species with much lower saturation vapor pressures compared to the precursor reactants[23]. For

example, the following classes of accretion reactions have been experimentally studied with respect to their role in SOA formation:[24]

ROOH (hydroperoxide) + R'CHO (aldehyde) ⇌ ROOCHR'OH (peroxyhemiacetal) (R1)

ROH (alcohol) + R'CHO (aldehyde) ⇌ ROCHR'OH (hemiacetal) (R2)

RCCOR' (carbonyl) + R"COR"' (carbonyl) ⇌ CR"R"'OHCRCR'O (aldol addition product) (R3)

RCO_2H (carboxylic acid) + R'OH (alcohol or carboxylic acid) ⇌ RCOR'O (ester or acid anhydride) + H_2O (R4)

$SO_2(OH)_2$ (sulfuric acid) + ROH (alcohol or gem-diol) ⇌ $SO_2(OH)(OR)$ (sulfate ester) + H_2O (R5)

These accretion reactions involve closed-shell organic compounds, in which all electrons are paired in their molecular orbitals to create stable and less reactive molecules. Therefore, such reactions, hereafter called closed-shell accretion reactions, have high energy barriers. Accretion reactions of the **R1**-**R5** type are therefore unlikely to occur in the gas phase, and most studies on their atmospheric relevance have accordingly focused on studying the condensed phase (e.g. cloud droplets).[25] In addition to closed-shell accretion reactions, also reactions involving radical species, as well as high-energy Criegee intermediates (carbonyl oxides) have been suggested to contribute to atmospheric SOA formation.[24] For instance, the reactions of stabilized Criegee intermediates ($RC(CH_3)(OO)$) with alcohol, water, carboxylic acid, etc., forming adducts of the general type ($RC(CH_3)(OR)(OOH)$) (**R6**) have attracted attention by experimentalists[24] and theoretical studies, such as ref 26, have recently addressed $RO_2 + RO_2 \rightarrow ROOR + O_2$ reactions. Accretion reactions may also occur in the gas phase. However, the detailed mechanisms are likely to be complex, and involve for example intersystem crossing. In this study, we focus on catalysis of closed-shell accretion reactions by small inorganic aerosol models. Catalysis of accretion reactions by single molecules or small molecular clusters can be considered as an intermediate case between gas-phase and condensed-phase chemistry, and has recently received increasing attention in atmospheric chemistry.[27-30] However, the central question of "which species are able to catalyze closed-shell accretion reactions?" has not yet been answered conclusively.

To find the species that can catalyze accretion reactions of closed-shell species, we have previously evaluated the effect of ammonia, water, formic acid and sulfuric acid clusters on six model reactions.[31] The results showed an increase in the rate of the reactions, but clarified that the studied clusters cannot catalyze the reactions sufficiently for the process to be competitive in the troposphere. Since mineral dust is abundant in atmospheric aerosols, and closed-shell accretion reactions are unlikely to occur in the gas phase,[24] we now investigate the intrinsic potential of mineral dust for catalyzing non-radical

accretion reactions. It should be noted that several experiments have been dedicated to unraveling the role of dust in oxidative formation of SOAs, e.g. refs 32,33. However, these studies have mainly analyzed and discussed the catalytic role of aged and unprocessed dust particles or surrogate minerals in dissociating ozone molecules and reducing oxidative SOA formation. Therefore, this study complements the information available on the effect of mineral dust on SOA formation. Due to the diversity of the organic compounds that can participate in SOA formation, this study narrows down the list of possible accretion reactions and focuses on the following model reactions:

CH_2O (formaldehyde) + syn-HCO_2H (formic acid) $\rightleftharpoons$ HCO_2CH_2OH (R7)

$CH_2O + H_2O \rightleftharpoons CH_2(OH)_2$ (methanediol) (R8)

CH_3OH (methanol) + syn-$HCO_2H \rightleftharpoons CH_3OCHO$ (methyl formate) + H_2O (R9)

The organic compounds participating in **R7** to **R9** represent the most common organic functional groups in atmospheric chemistry. Furthermore, reactions **R7** to **R9** are relevant for tropospheric accretion product formation since carbonyls[14], alcohols and acids[34-36] have all been identified as important precursors for SOAs[5]. To determine the impact of dust aerosols on reactions **R7** to **R9**, a chemical kinetics approach is followed. We first explore the reaction mechanisms in the absence and presence of dust aerosols. Next, the impact of mineral dust is quantified by calculating the rate constants of the reactions in the gas phase, and on the surface of dust, using transition state theory under representative tropospheric conditions.

2. METHODS

2.1. Computational Details

Gaussian 16 revision A.03[37] was employed to perform all density functional theory (DFT)-based calculations. The geometry optimizations and harmonic frequency calculations were executed using the ωB97X-D density functional[38] with the 6-31++G** basis set. The ωB97X-D functional was specifically used due to the importance of electrostatic long-range exchange-correlation and relative significance of electrostatic correction[39] for the study of the reactions between closed-shell compounds. Moreover, the ωB97X-D functional has been shown to describe noncovalent interactions precisely and give accurate thermochemical and chemical kinetics results[38,40].

Further, *ab initio* single point energy calculations were applied to the optimized geometries to increase the accuracy of the final energy profiles. For this purpose, the domain-based local pair-

natural orbital (DLPNO)-CCSD(T) method[41-43] was chosen since it has been shown to be an efficient, cost-effective and accurate method for analyzing thermochemistry of closed-shell organic molecules[44] providing results close to those of canonical coupled cluster calculations[45]. Along with the DLPNO-CCSD(T) method, the aug-cc-pVTZ[46,47] basis set, the cc-pVTZ/C auxiliary basis and the tight pair natural orbital (TightPNO) criterion were used. Using the standard notation of quantum chemistry, the reaction profiles were thus described at the DLPNO-CCSD(T)/aug-cc-pVTZ//ωB97X-D/6-31++G** level of theory. Since the DLPNO-CCSD(T) method is not implemented in Gaussian, Orca 4.1.1[48] was used for the corresponding energy calculations. Calculating single point coupled-cluster electronic energies for DFT-optimized geometries is a standard approach in computational chemistry, both in atmospheric applications and elsewhere[49,50].

Benchmarking of the selected level of theory was addressed in our previous study[31] by comparing the Gibbs free energy and activation energies of seven accretion reactions with the values obtained from the high *ab initio* level of CCSD(T)-F12/VTZ-F12//MP2/aug-cc-pVTZ. The comparison yielded the mean absolute error (MEA) error of 2.3 kJ mol^{-1} for DLPNO-CCSD(T)/aug-cc-pVTZ//ωB97X-D/6-31++G**. The suitability of the computational level was further confirmed by comparing the geometries optimized at the ωB97X-D/6-31++G** level with the available experimental geometries of the reactants and products and, also, the geometries obtained from several computational levels (see Figure S1). Furthermore, the enthalpy of the reactions at 0 K was compared with the available experimental data in Table S1. Both Figure S1 and Table S1 demonstrated appropriateness of the selected level for study of reactions **R7** to **R9**.

After validating the computational approach, the reaction mechanisms were explored at the ωB97X-D/6-31++G** level. The stationary structures with non-imaginary frequencies were assigned as reaction intermediates/wells while the structures with an imaginary frequency were tentatively assigned as transition states (TS). To verify the identity of the TSs, as well as their corresponding reactants and products, intrinsic reaction coordinate (IRC)[51,52] calculations were performed in both forward and reverse directions. The energy profiles of the resultant reaction paths were obtained by combining the DLPNO-CCSD(T)/aug-cc-pVTZ electronic energies with the ωB97X-D/6-31++G** vibrational zero-point energies (ZPE) energies for all stationary points.

In the case of the surface-based reactions, the reactants could approach the dust models in many ways. To screen the possible reactant/dust complexes, the artificial bee colony (ABC) algorithm, as embedded in the ABCluster 1.4 program[53,54], was employed. Using the ABC algorithm, 500 initial reactant/dust configurations were created as the trial population. Each trial structure was adopted as a starting point to generate 500 new structures and search for the local and global minima structures

using 10 scout bees. The energy of each generated complex was considered as the sum of Lennard-Jones and Columbic interactions to give a list of 200 structures as the local minima for each reactant/dust complex. In the next step, the generated local minima were optimized using the GFN-xTB[55] semi-empirical method by the XTB 6.0.1 program[56]. After that, the structures were sorted based on their Gibbs free energy values at 298 K, and the 30 lowest-energy structures for each reaction were re-optimized at the ωB97X-D/6-31++G** level of theory. The most stable structures from this optimization process were then used to scan the possible reaction paths (see Figure 1 for the global minima (GM) structures of the surface-based reactions related to the smallest dust model). However, in the case of **R7** on the smallest model, the GM complex was so stable that forcing the reactants to approach each other ended up with reactant decomposition. Consequently, the corresponding reaction path was deemed to be unfavorable, and the less stable complexes were tested to find the representative pre-reaction complexes and the related TSs.

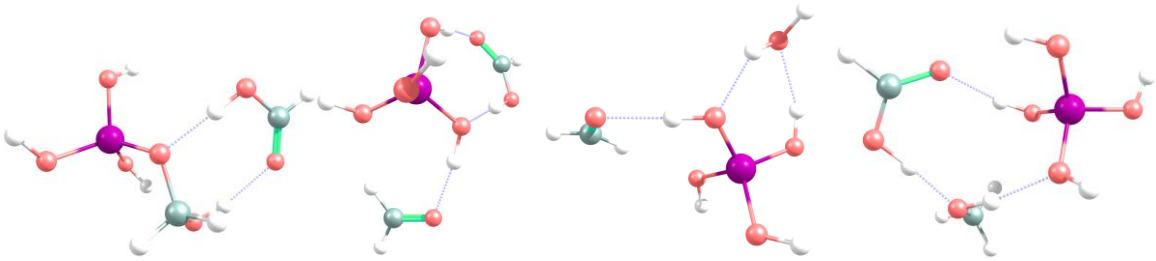

GM(M)-FFA (R7) **RC3(M)-FFA (R7)** **GM(M)-FW (R8)** **GM(M)-FAM (R9)**

Figure 1. The GM structures of the reactants/dust model clusters. The purple, red, grey and white balls represent silica, oxygen, carbon and hydrogen, respectively.

2.2. Mineral Dust Model Selection and Validation

To evaluate the impact of mineral dust on the studied reactions, an appropriate model dust structure is required. Such a structure is not straightforward to generate, as the structure and chemistry of dust aerosols are highly complex and variable. The composition of dust aerosols depends on their sources[57]. Also, their chemical and physical properties change upon aging[58,59] and phase transitions[58]. Moreover, the distribution of mineral components in dust is naturally inhomogeneous,[60] and mineral components may have different particle sizes[60,61]. To simplify the problem, we focused on the major dust minerals. Based on numerous studies on dust components, quartz is the major oxide component of mineral dust (40% to 70%)[62,63]. In addition, quartz has been reported as a significant component of different dust samples, e.g. see refs 60,64-67. Also, feldspars (aluminosilicates) have been shown to contribute considerably to diverse dust samples[63,67-69]. These two classes of minerals form over

80% of the volume of mineral dust[70]. Besides quartz and feldspars, significant amounts of calcite[63,64,67,69] and clays (such as kaolinite[60,63,69] and illite[68]) have been observed in many dust samples. However, their relative amounts are significantly lower than those of feldspars and quartz.[67] It should be also noted that molten clays can transform into feldspars as they mostly consist of phyllosilicates[60]. Our model dust minerals were thus assumed to contain only feldspars and quartz. Since these minerals are mainly composed of silica (SiO_2) units, and closed-shell reactions between neutral molecules require the reactants to be in close proximity to each other, a small silica model should be sufficient for representing mineral dust aerosols. Accordingly, mono-silicic acid (Mcat, $Si(OH)_4$) was chosen as the basic model of mineral dust. To investigate the effect of dust model size on our results, linear tri-silicic acid (Tcat, $Si_3O_2(OH)_8$) was also considered, as suggested by Ji et al.[62]. Though silicic acid has been accepted as the best geometrical and chemical model of SiO_2 minerals[62,71-73], the model choices were further validated by comparing their optimized geometries with several quartz, feldspar and clay crystal structures (see Table S2). Based on the geometrical parameters outlined in this table, both Mcat and Tcat can capture the general geometrical features of silica-based minerals. Therefore, they were chosen to represent dust aerosols.

3. RESULTS AND DISCUSSION

Reaction mechanism

To understand the effect of mineral dust on closed-shell accretion reactions, the mechanism of reactions **R7** to **R9** was first explored in the gas phase. Figures 2 to 4 show the potential energy surfaces (PESs) and Figures S2 to S4 present the geometries of the corresponding stationary points. It should be noted that, in these figures, the stationary points (reactant complexes and transition states) involved in reaction **R7** (the reaction between formaldehyde and formic acid; F and FA) are distinguished by including the acronym "FFA" in their names, while the names of the stationary points involved in reaction **R8** (the reaction between formaldehyde and water; F and W) contain "FW", and those of reaction **R9** (the reaction between formic acid and methanol; FA and M) contain "FAM". Also, numerical identities have been attributed to all stationary points to distinguish between the species related to each reaction.

As seen in Figures 1-3, the entrance channels of all three reactions are barrierless. This means that when the reactants are at large separations, they should be able to overcome the centrifugal barrier to approach each other, and form a pre-reaction complex, at rates comparable to the gas-kinetic collision rate. The generated pre-reaction complexes can then pass over TS-FFA (19.7 kJ mol^{-1}) and TS-FW

(152.4 kJ mol^{-1}) (see Figure 5 for their structures) to give the final products of reactions **R7** and **R8**, respectively. In the case of **R9**, the reaction can follow two different paths to produce the accretion products. Along the first path, the pre-reaction complex undergoes intermolecular hydrogen transfer from the -OH group of methanol to the carbonyl oxygen (O=C) of formic acid, simultaneous with the formation of a C-O bond between the two reactants (TS1-FAM; 132.6 kJ mol^{-1}), producing the INT intermediate (-14.8 kJ mol^{-1}) (see Figures 5 and S4 for the geometries). Next, internal hydrogen transfer from one hydroxyl group of INT to another, together with gradual cleavage of the O-H bond of the hydrogen receptor hydroxyl group (TS2-FAM; 142.5 kJ mol^{-1}), yields water and CH_3OCHO. Along the second path, the hydrogen from the hydroxyl group of methanol is directly transferred to the hydroxyl group of formic acid, simultaneous with the formation of a C-O bond between the two reactants, and cleavage of the O-H bond in formic acid (TS3-FAM; 158.9 kJ mol^{-1}). This results in a weakly bound post-reaction complex which later dissociates into the individual water and CH_3OCHO products.

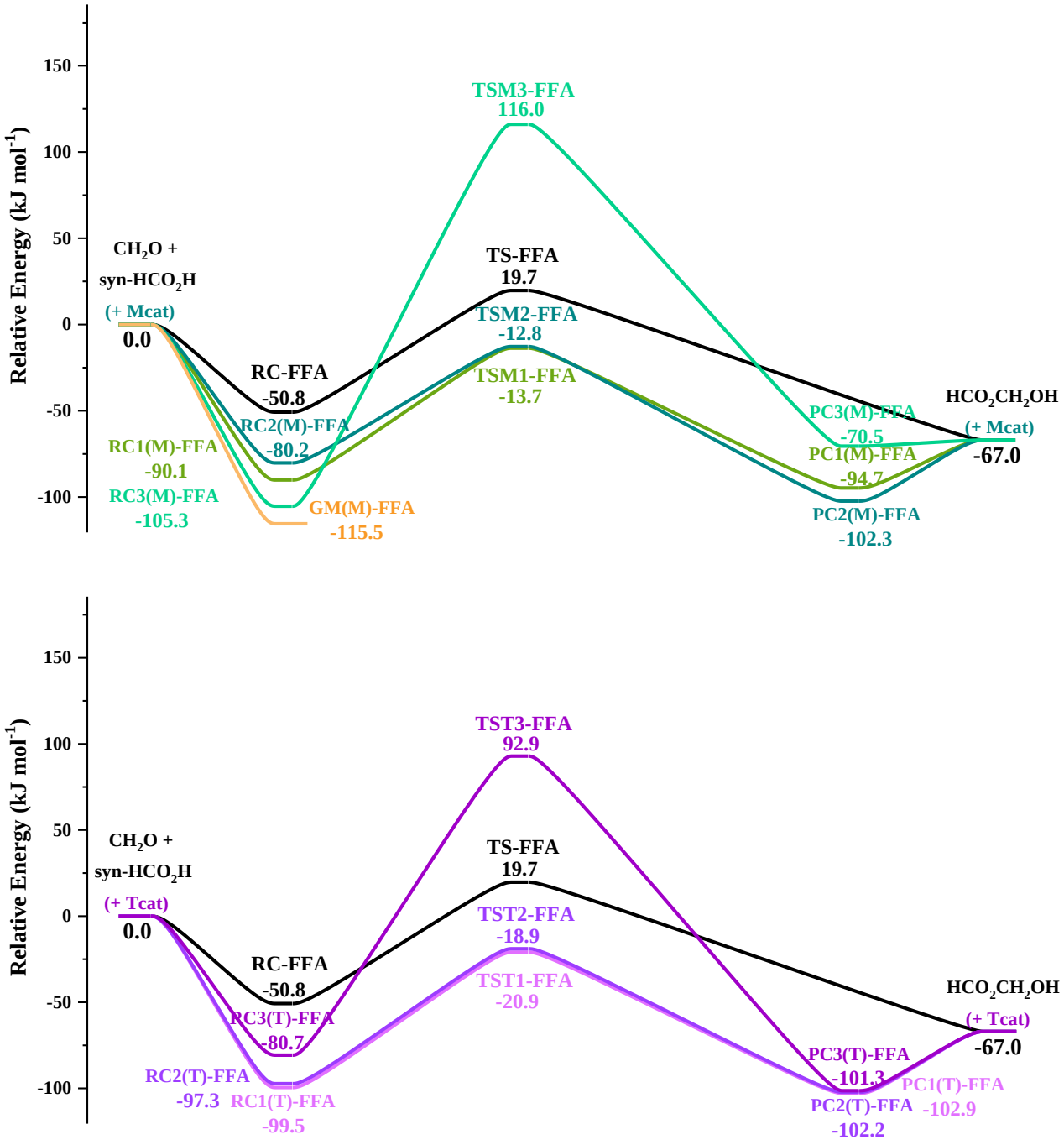

Figure 2. The ZPE-corrected potential energy surface of **R7** at the DLPNO-CCSD(T)/aug-cc-pVTZ//ωB97X-D/6-31++G** level of theory and 0 K. The black, green and purple reaction paths refer to the gas-phase, Mcat-based and Tcat-based reactions, respectively.

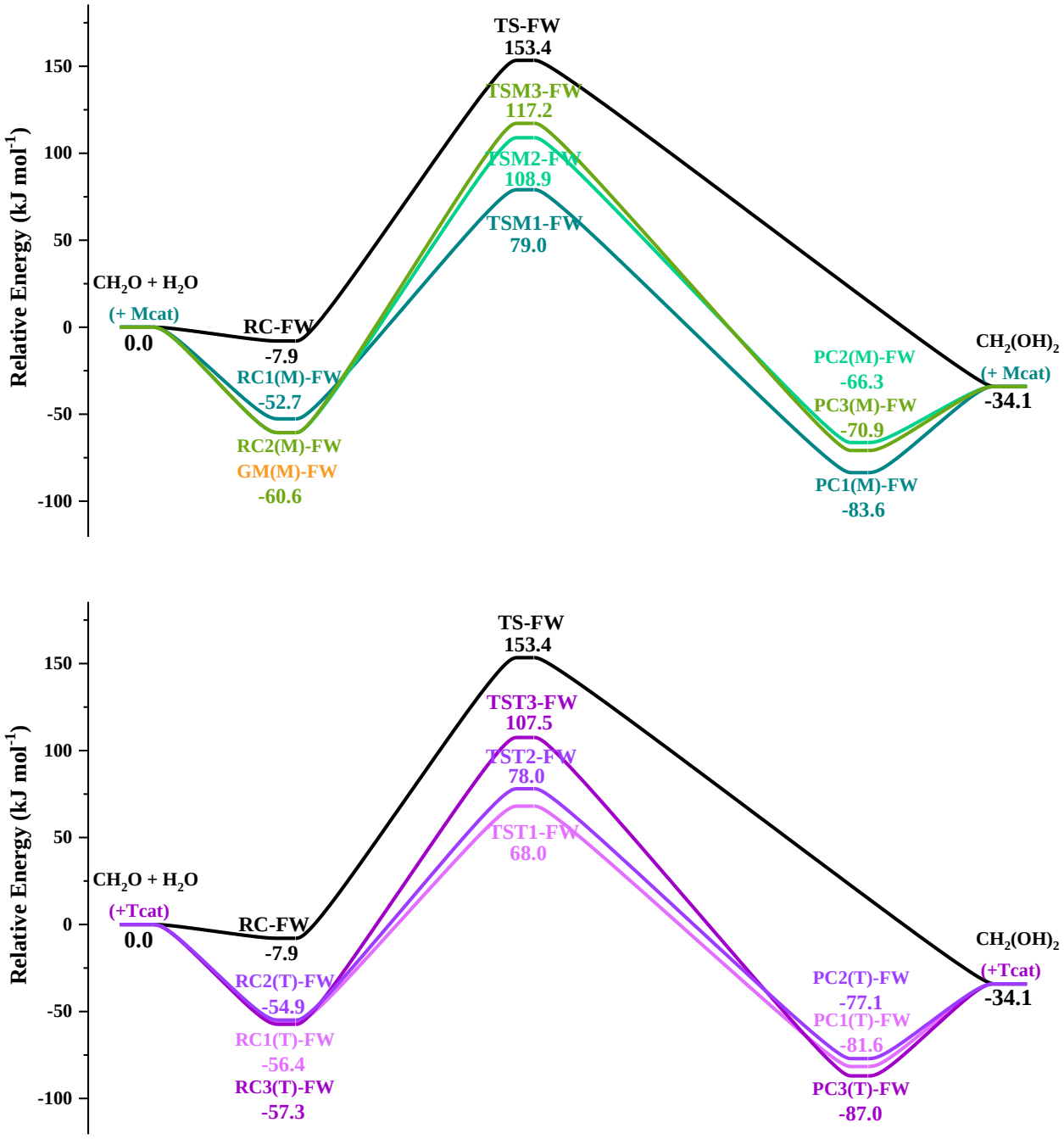

Figures 3. The ZPE-corrected potential energy surface of **R8** at the DLPNO-CCSD(T)/aug-cc-pVTZ//ωB97X-D/6-31++G** level of theory and 0 K. The black, green and purple reaction paths refer to the gas-phase, Mcat-based and Tcat-based reactions, respectively.

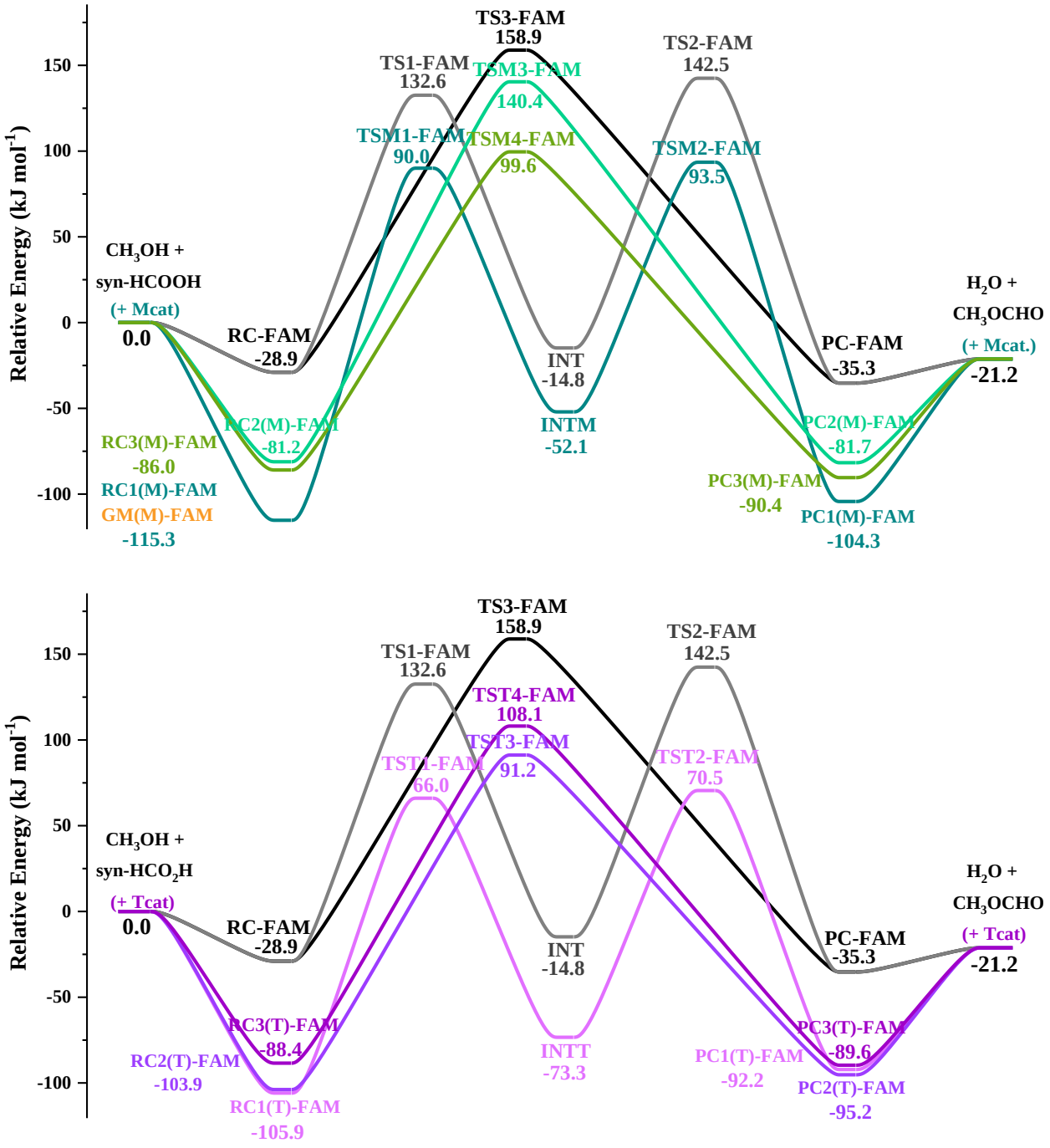

Figures 4. The ZPE-corrected potential energy surface of **R9** at the DLPNO-CCSD(T)/aug-cc-pVTZ//ωB97X-D/6-31++G** level of theory and 0 K. The black (and grey), green and purple reaction paths refer to the gas-phase, Mcat-based and Tcat-based reactions, respectively.

Regardless of their detailed mechanisms and energy profiles, the gas-phase reactions **R7** to **R9** share two general features: they all involve relatively stable pre-reaction complexes, and their rates are limited by high reaction barriers. The apparent barrier heights, i.e. the barrier energies relative to the

free reactants, range from 19.6 (TS-FFA; **R7**) to 158.9 (TS3-FAM; **R9**) kJ mol^{-1}, at 0 K. A close look at the structures of the TSs (see Figure 5), suggests that the strain caused by formation of ring-like geometries destabilizes the TSs,[31] while hydrogen bonding stabilizes them. This hypothesis is supported by comparing the geometry of TS-FFA with a 6-membered ring and the lowest barrier height (19.6 kJ mol^{-1}) to the geometry of the other TSs with 4-membered rings and barrier heights above 130 kJ mol^{-1}.

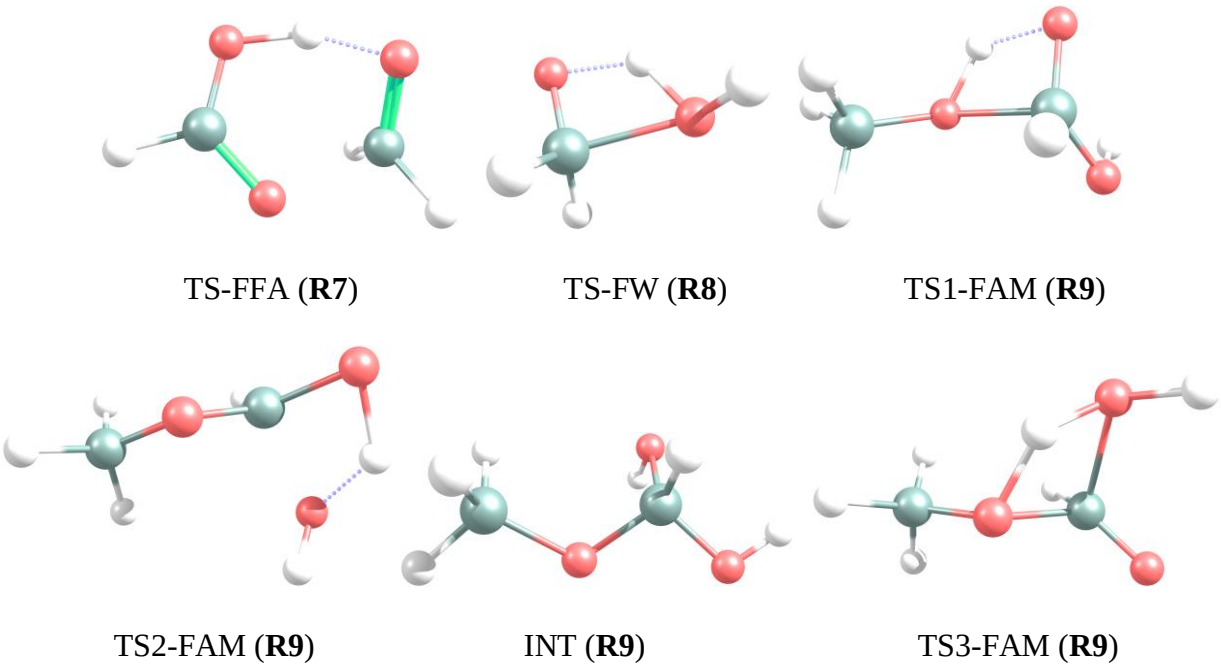

Figure 5. Transition state geometries of gas-phase **R7** to **R9** reactions. The blue dotted lines represent hydrogen bonding. The red, grey and white balls represent oxygen, carbon and hydrogen, respectively.

The fundamental question of this study concerns the effect of mineral dust on the reactions. Therefore, the reaction mechanisms were also investigated in the presence of the mineral dust models. To facilitate distinguishing the stationary points of the dust assisted and gas phase reactions, (M) or M is added to the notation of the Mcat-based reactions. Similarly, (T) and T in the notation refer to the Tcat-based reactions. When Mcat is added to the reactive system, the reactants can form hydrogen bonds with the hydroxyl groups of Mcat. See Figures S2 to S4 for illustrations of all pre-reaction geometries, and Figure 6 for the pre-reaction complexes of reaction **R7**, which are very close in energy, but involve different orientations of the reaction products. The additional hydrogen bonds stabilize the reactant complexes to a much greater extent compared to the gas-phase reaction (see Figures 2 to 4).

After forming the pre-reaction complexes, two factors determine the fate of the adsorbed reactants: the extent of stabilization, and the relative orientation of the reactants. Figures 2 and 6 illustrate this, and show that the well-oriented reactants in the pre-reaction complexes RC1(M)-FFA and RC2(M)-FFA (Mcat-based **R7**) can easily convert into products by passing over the submerged barriers corresponding to transition states TSM1-FFA and TSM2-FFA, which are respectively 13.7 and 12.8 kJ mol^{-1} below the energy level of the free reactants at 0 K. However, in the RC3(M)-FFA complex, the two reactants are stabilized by different hydroxyl groups. This inappropriate orientation causes their large separation, leads to a very high energy barrier (TSM3-FFA; 116.0 kJ mol^{-1} above the free reactants). It should be noted that TSM3 is 96.3 kJ mol^{-1} higher than the gas-phase barrier (TS-FFA), while TSM1 and TSM2 are 33.4 and 32.5 kJ mol^{-1} lower than the gas-phase barrier, respectively. In the case of **R8** and **R9**, Mcat reduces the barrier of all reaction paths by about 18.5 to 74.4 kJ mol^{-1}.

According to the outlined energy profiles, the performance of dust minerals in surface-based accretion reactions strongly depends on the starting configurations of the reactants/Mcat clusters. The different orientations of the reactants toward the surface and each other create multiple reaction paths with highly variable barriers. Along some reaction paths, mineral dust may inhibit the reaction due to the inappropriate relative orientation of the reactants in the reactant complexes. On the other hand, along some reaction paths, the favorable orientation of reactants on mineral dust assists the conversion of reactants into the products. The combination (and competition) of these two determines whether or not mineral dust acts as a catalyst for a particular reaction. In any case, the surface hydroxyl groups of dust minerals are predicted to have a noticeable role in stabilization of the reactants. They also stabilize the reaction products by forming post-reaction complexes, and also increase the stability of the INT intermediate for **R9**. It should be noted that in the gas-phase, our calculations predict the existence of a post-reaction complex only for **R9**.

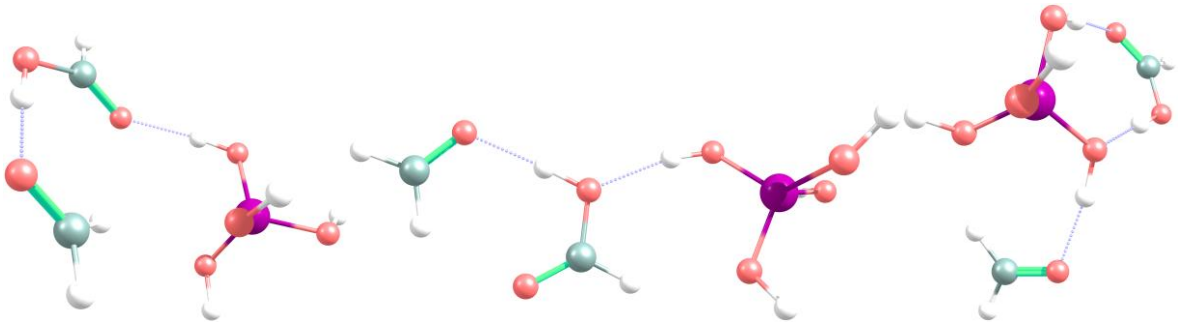

RC1(M)-FFA RC2(M)-FFA RC3(M)-FFA

Figure 6. Pre-reaction complexes of Mcat-based reaction of formaldehyde with formic acid (**R7**). The blue dotted lines represent hydrogen bonding. The silica, oxygen, carbon and hydrogen atoms are respectively shown as purple, red, grey and white balls.

The reaction mechanisms were also evaluated in the presence of Tcat to analyze the effect of a larger dust unit with more accessible silica atoms and hydroxyl groups. As illustrated by Figures 2 to 4, access to more adsorption sites, i.e. more hydroxyl groups, affects the energies of the various pre- and post-reaction complexes in different ways. Some pre- and post-reaction complexes are less stable than their Mcat-based counterparts, while the others are more stable. Another general feature of the Tcat-based reactions is that many of the related pre- and post-reaction complexes have similar relative energies, e.g. RC1(T)-FFA and RC2(T)-FFA (**R7**), PC1(T)-FFA and PC2(T)-FFA (**R7**), RC1(T)-FW, RC2(T)-FW and RC3(T)-FW (**R8**), RC1(T)-FAM and RC2(T)-FAM (**R9**). However, they have distinguishable structures as shown in Figures 6 and S2 to S4. Despite variations in the relative energies and configurations of the pre-reaction complexes, the use of Tcat lowers the overall barrier heights in all cases. Also, INT (-14.8 kJ mol^{-1}; **R9**) can be noticeably stabilized by Tcat (INTT: -73.3 kJ mol^{-1}) compared to Mcat (INTM: -52.1 kJ mol^{-1}). In general, Tcat acts more effective than Mcat in reducing the barrier heights, which means that larger mineral dust catalytic sites are more effective than the smaller sites in assisting the progress of the studied accretion reactions.

3.2. Catalytic Efficiency in the Troposphere

The detailed PESs reported in Figures 2 to 4 are not sufficient for determining the catalytic role of mineral dust in atmospheric conditions since the presented energy profiles ignore thermal and entropic contributions. Also, the overall atmospheric importance of the catalytic reactions depends on the concentration of catalytic sites. To quantitatively estimate the effect of mineral dust on the extent of the studied accretion reactions, the rates of the surface-based and gas-phase reactions under tropospheric conditions should be calculated. The rate expressions of the reactions were written in the general form of eq 1, where *k* is the total rate constant of the reaction, squared brackets denote concentrations, and the number of "reactants" *m* equals 2 for gas-phase reactions, and 3 for the surface-based reactions (where the catalyst is included as a "reactant" for the purpose of evaluating the rate).

$$rate = k \times \prod_{i=1}^{m} [(reactant)_i] \quad (1)$$

To determine if mineral dust can really catalyze the studied accretion reactions, we define the catalytic enhancement (*C.E.*) parameter as the ratio of the catalyzed reaction rate to the gas-phase rate.[74] In adopting this definition, we implicitly assume that the kinetics of the surface-based reactions is controlled by the chemical reaction rather than the diffusion process of reactants to the surface. This means that we assume that the same concentration of water, formaldehyde, formic acid and methanol reactants are available for both gas-phase and surface-based reactions. Under this assumption, the

enhancement of the accretion reactions only depends on the concentration of Mcat or Tcat, and the *k* values of the gas-phase and surface-based reactions. To calculate the rate coefficients of the reactions, tunneling-corrected transition state theory was applied to the PESs, yielding the following expression:

$$k = \kappa_r \times \frac{k_\beta T}{h} e^{-\Delta_r^\# G / RT} \quad (2)$$

In this equation, κ_r is the tunneling coefficient, k_B is the Boltzmann constant, h is the Plank constant, T is temperature, R is the universal gas constant and $\Delta_r^\# G$ is the difference between the Gibbs free energy of the corresponding TS (G_{TS}) and the free reactants ($G_{reactants}$), see eq 3 for details. Note that for the surface-based reactions, the free "reactants" include Mcat or Tcat. The tunneling effect is specifically emphasized in eq 2 since the tropospheric reactions take place at temperatures below 300 K, where tunneling may be important especially for reactions involving the motion of hydrogens or protons. To calculate κ_r, the reaction barriers were described as unsymmetrical Eckart barriers[75]. Our kinetic treatment implicitly assumes that the reactants are in equilibrium with the pre-reaction complexes, and that the different pre-reaction complexes can interconvert into each other (see Table S3 for the Gibbs free energies of the pre- and post-reaction complexes). Under such condition, the exact energies of the pre-reaction complexes do not affect the rate constants of the reactions.[74] Note that neglecting the pre-reaction complexes or using the steady state approximation and including the conversion of the pre-reaction complexes to the post-reaction complexes, as done in ref 76, gives the same final rate constant equation. Also, in the case of the two-step reaction path of **R9**, the rate determining step was assumed to be the TS with the highest absolute G_{TS}. To be more specific, TS2-FAM, TSM2-FAM and TST2-FAM were identified as the rate-determining barriers on the two-step paths of the gas-phase, Mcat- and Tcat-based **R9** reactions, respectively. To obtain the *G* values of the species at the DLPNO-CCSD(T)/aug-cc-pVTZ//ωB97X-D/6-31++G** (DLPNO-DFT) level of theory, the electronic energy obtained from single point energy calculation at the DLPNO-CCSD(T)/aug-cc-pVTZ level (E_{DLPNO}) was summed with the thermal contribution to Gibbs free energy retrieved from the ωB97X-D/6-31++G** frequency calculations ($G_{thermal}^{DFT}$) (eq 4):

$$\Delta_R^\# G = G_{TS} - G_{reactants} \quad (3)$$

$$G_{DLPNO\text{-}DFT} = E_{DLPNO} + G_{thermal}^{DFT} \quad (4)$$

Finally, implementing eq 2 for all possible reaction paths in our definition of *C.E.* resulted in the following general equation:

$$C.E. = \frac{[catalyst]}{\kappa_{r0}} \sum_{i=1}^{n} \kappa_{ri} \times e^{\left(\Delta_{r0}^\# G - \Delta_{ri}^\# G\right)/RT} \quad (5)$$

Here, the subscripts "ri" and "r0" denote the surface-based and gas-phase reactions, respectively, for all *n* reaction paths, and *C.E.* can be considered dimensionless by expressing catalyst concentration as the ratio of catalyst pressure in the atmosphere to the reference pressure used in the $\Delta_r^{\#}G$ calculations (1 atm), which makes the ratio *C.E.*/[catalyst] a dimensionless number. Table S4 reports the $\Delta_r^{\#}G$ and κ_r values of the **R7**, **R8** and **R9** reaction paths computed at 198 and 298 K (1 atm) and embedded in eq 5. Based on Table S4, the tunneling effect is more profound in the case of the gas-phase reactions, and at the lower temperature of 198 K, as expected. In addition, tunneling varies significantly from one reaction path to another due to the differences in the barrier heights and the associated imaginary frequencies. The combined effect of the variations in barrier height, imaginary frequency and temperature leads to κ_r values ranging from 1.88 to 8.02.

A fact highlighted by Table S4 is that the energy profiles of the studied reactions are quite sensitive to the thermal contributions. For example, for the surface-based **R7** reaction paths, the TSs are below the reactants according to their ZPE-corrected energies, but above the reactants in terms of free energy at 298 K. On the other hand, the thermal contribution is not sufficient at 198 K to raise the TSs above the reactants. The thermal contribution at 198 K is naturally lower than that of 298 K also for **R8** and **R9**. Interestingly, along some reaction paths of **R8** and **R9**, consideration of thermal contribution gives surface-based reaction barriers that are lower than the barrier of the gas-phase reactions, see for example the "r1 (TSM1-FW)" reaction path of **R8** at 298 K in Table S4. Table S4 also shows that mineral dust catalysis reduces the enthalpy barriers of the reactions ($\Delta_r^{\#}H$) along most reaction paths, which is not surprising as enthalpy and ZPE-corrected electronic energy are similar to each other. However, as adsorption of the reactants on the surface of mineral dust limits their translational freedom, the entropy of the reactions ($\Delta_r^{\#}S$) decreases on the surface of Mcat and Tcat, and the reactions become entropically less favorable. In the case of **R7** and **R9** (both at 298 K), the decrease of enthalpy does not compensate for the negative effect of entropy reduction, while the decrease of enthalpy can compensate for the impact of entropy reduction for **R7** (198 K), **R8** (198 and 298 K) and **R9** (198 K).

Since *C.E.* depends on the $\Delta_r^{\#}G$ and κ_r values (see eq 5), the discussed thermochemical changes are reflected in the *C.E.*/[catalyst] results, which are outlined in Table 1. If we ignore the effect of catalyst concentration and just focus on the *C.E.*/[catalyst] values, mineral dust seems to be able to catalyze all three reactions at 198 K. However, the *C.E.*/[catalyst] values clearly show that both Mcat and Tcat inhibit **R7** at 298 K by elevating the reaction barrier. The *C.E.*/[catalyst] results also show that Tcat outperforms Mcat in lowering the barrier height for all reactions and, therefore, increasing the rate of all studied reactions. Therefore, if we just rely on the *C.E.*/[catalyst] results, mineral dust would seem

to be able to catalyze all reactions at 198 K, and thus enhance SOA formation. In particular, the *C.E.*/[catalyst] values suggest that each Tcat site can catalyze the **R8** reaction up to a factor of 9.64×10^{5} and 4.35×10^{13} at 298 and 198 K, respectively. The *C.E.*/[catalyst] values of **R7** and **R9** are also higher at 198 K. In other words, based on the *C.E.*/[catalyst] results, mineral dust seems to enhance the accretion reactions more significantly at higher altitudes in the troposphere, where the temperature is lower. Furthermore, *C.E.*/[catalyst] results would indicate that, at lower altitudes (298 K), dust aerosols would act more selectively by retarding **R7** while enhancing **R8** and **R9**. It should be added that neither the *C.E.* nor the *C.E.*/[catalyst] values depend significantly on the number of the reaction paths offered by the dust surface, as some reaction paths are far less feasible than the others – *C.E.* is dominated by the most favorable path (highest rate coefficient *k*).

Finally, we estimated the catalyst concentrations ([Mcat] and [Tcat]) in order to determine whether catalysis of accretion reactions by mineral dust is an important process in the real atmosphere. For this purpose, we defined [Mcat] and [Tcat] as the number concentration of the catalytic sites (number of Mcat or Tcat sites per volume of air). To find an appropriate range of values, the typical surface area concentration of dust aerosol was taken to be 1.0×10^{-6} - 1.0×10^{-7} cm^2 cm^{-3}, according to the values reported in refs 77-80. Then, the total number of active sites present in the tropospheric dust aerosols per unit volume of air (i.e. [catalyst]) was obtained by dividing this total surface area concentration of mineral dust aerosols by the surface area of Mcat (25.76 $Å^2$) or Tcat (55.33 $Å^2$) (calculated using ChemCraft 1.8 [81]). The resultant catalyst concentrations (in cm^{-3}, which should be interpreted as the number of catalytic sites per cm^3 of air) were then converted into the unit of atm by applying the ideal gas law. As presented in Table 1, the *C.E.* values are below 10^{-3} for all reactions and reaction conditions, which shows that mineral dust aerosols cannot contribute significantly to the progress of atmospheric accretion reactions of closed-shell compounds. It should be added that the relatively low concentration of catalytic sites in the troposphere is not the only reason behind the negligible *C.E.* values. Another important reason is that the bimolecular *k* values of many of the studied gas-phase and surface-based reaction paths are lower than 10^{-37} cm^3 $molecule^{-1}$ s^{-1}, under tropospheric conditions, with only a few of the **R7** reaction paths reaching *k* values above 10^{-20} cm^3 $molecule^{-1}$ s^{-1}. Thus, even if the relative enhancement of the rates due to the presence of mineral dust is in some cases enormous, the absolute reaction rates are still extremely slow in an atmospheric chemistry context.

Table 1. The *C.E.*/[Mcat or Tcat] and Estimated *C.E.* Values of R7, R8 and R9 in the Presence of Mcat and Tcat at Atmospherically Representative Concentrations of Catalyst Sites per Unit Volume

	C.E./[Mcat or Tcat]		*C.E.*	
	298.15 K	198.15 K	298.15 K	198.15 K
R7 (Mcat)	2.35×10^{-2}	1.92×10^{1}	3.61×10^{-20} - 3.61×10^{-19}	1.95×10^{-17} - 1.95×10^{-16}
R7 (Tcat)	3.33×10^{-1}	8.87×10^{2}	2.38×10^{-19} - 3.61×10^{-18}	4.20×10^{-16} - 4.20×10^{-15}
R8 (Mcat)	1.05×10^{4}	7.18×10^{10}	1.61×10^{-14} - 1.61×10^{-13}	7.31×10^{-8} - 7.31×10^{-7}
R8 (Tcat)	9.64×10^{5}	4.35×10^{13}	6.87×10^{-13} - 6.87×10^{-12}	2.06×10^{-5} - 2.06×10^{-4}
R9 (Mcat)	5.36×10^{-1}	1.41×10^{4}	8.21×10^{-19} - 8.21×10^{-18}	1.43×10^{-14} - 1.43×10^{-13}
R9 (Tcat)	7.17×10^{2}	1.98×10^{9}	5.11×10^{-16} - 5.11×10^{-15}	9.40×10^{-10} - 9.40×10^{-9}

4. CONCLUSIONS

To find the atmospheric species or particles that might catalyze formation of secondary organic aerosols in the troposphere, we investigated the role of mineral dust in dimerization kinetics of model closed-shell organic compounds (**R7** to **R9**). By analyzing the reaction mechanism at 0 K, mineral dust was found to have the potential for enhancing adsorption of the reactants, directing them toward pre-reaction complex formation, reducing the barrier heights and stabilizing the post-reaction complexes. This would strongly increase the formation rate of dimers which are less volatile than the original organic compounds. However, inclusion of thermal effects (using a temperature range of 198 K to 298 K relevant to the troposphere) leads to a significant decrease in the predicted catalytic effect due to the entropy penalty associated with clustering of the reactants with the catalytic sites. The magnitude of this penalty increases with temperature, and thus opposite to altitude in the troposphere.

If the effect of catalyst (dust aerosol) concentration be neglected, dust aerosols would enhance the reaction of water and formaldehyde in the lower part of the troposphere (with temperatures close to 298 K). In contrast, dust particles tend to inhibit the reaction of formaldehyde with formic acid. The reaction of methanol with formic acid at 298 K is only enhanced if a sufficient number of silica bound hydroxyl groups be available for stabilizing the reacting species. In the upper troposphere (with temperatures closer to 198 K), mineral dust is able to enhance all three studied reactions. In particular, mineral dust would have a drastic impact on the reaction of water with formaldehyde toward $CH_2(OH)_2$ production if a sufficient amount of mineral dust aerosols be available. In other words, **R8** would have the greatest contribution to SOA formation in the presence of abundant mineral dust catalytic sites.

Further, the inherent catalytic effect of reactions **R7** (formaldehyde reaction with formic acid), **R8** (formaldehyde reaction with water) and **R9** (formic acid reaction with methanol) were also calculated

for molecular clusters of water (**R7**: 4.05×10^{-2} and **R8**: 1.37×10^{8}) and sulfuric acid (**R7**: 2.39×10^{6}, **R8**: 7.08×10^{24} and **R9**: 7.43×10^{22}) at 298 K, without including tunneling effects, based on the data of ref 31. The calculations revealed that when catalyst concentrations are neglected, sulfuric acid outperforms both mineral dust (Tcat; **R7**: 3.13×10^{-1}, **R8**: 9.64×10^{5} and **R9**: 7.17×10^{2}) and water in increasing SOA formation through accretion reaction of the studied closed-shell organic compounds.

Finally, the reactions were analyzed in a more realistic context by including the likely concentration range of active mineral dust sites in the atmosphere, allowing an estimation of the absolute values for the catalytic effect (*C.E.*). This analysis revealed that dust aerosols are not capable of contributing to atmospheric SOA formation through accretion reactions. The reasons for this are the insufficient concentration of active sites, and the relatively low absolute rate constants of the surface-based reactions. In contrast, sulfuric acid at atmospheric concentrations of around 1×10^{6} molecule cm^{-3} [82] is indeed able to enhance some closed-shell accretion reactions (*C.E.*; **R7**: 9.43×10^{-14}, **R8**: 2.79×10^{5} and **R9**: 2.93×10^{3}).

Supporting Information

The Cartesian coordinates and the geometries of the silica models, reactants, products, transition states and reaction complexes, reaction enthalpies at different level of theory, the imaginary frequencies of the transition states, the tunneling coefficients, the reaction Gibbs free energies and the output files for single-point energy and frequency calculation on all structures.

ACKNOWLEDGEMENTS

We thank the Academy of Finland University of Helsinki, Faculty of Science ATMATH Project and the ERC Project 692891-DAMOCLES for funding and the CSC-IT Center for Science in Espoo, Finland, for computational resources.

REFERENCES

(1) Carlton, A. G.; Wiedinmyer, C.; Kroll, J. H. A Review of Secondary Organic Aerosol (SOA) Formation from Isoprene. *Atmos. Chem. Phys.* **2009**, *9*, 4987-5005.

(2) Novakov, T.; Penner, J. E. Large Contribution of Organic Aerosols to Cloud-Condensation-Nuclei Concentrations. *Nature* **1993**, *365*, 823-826.

(3) Andreae, M. O.; Crutzen, P. J. Atmospheric Aerosols: Biogeochemical Sources and Role in Atmospheric Chemistry. *Science* **1997**, *276*, 1052-1058.

(4) Pope III, C. A.; Ezzati, M.; Dockery, D. W. Fine-Particulate Air Pollution and Life Expectancy in the United States. *New Engl. J. Med.* **2009**, *360*, 376–386.

(5) Kalberer, M.; Paulsen, D.; Sax, M.; Steinbacher, M.; Dommen, J.; Prevot, A. S. H.; Fisseha, R.; Weingartner, E.; Frankevich, V.; Zenobi, R.; Baltensperger, U. Identification of Polymers as Major Components of Atmospheric Organic Aerosols. *Science* **2004**, *303*, 1659-1662.

(6) Geddes, S.; Zahardis, J.; Petrucci, G. A. Chemical Transformations of Peptide Containing Fine Particles: Oxidative Processing, Accretion Reactions and Implications to the Atmospheric Fate of Cell-Derived Materials in Organic Aerosol. *J. Atmos. Chem.* **2009**, *63*, 187-202.

(7) Kanakidou, M.; Seinfeld, J. H.; Pandis, S. N.; Barnes, I.; Dentener, F. J.; Facchini, M. C.; Dingenen, R. V.; Ervens, B.; Nenes, A. N. C. J. S. E.; Nielsen, C. J.; Swietlicki, E. Organic Aerosol and Global Climate Modelling: A Review. *Atmos. Chem. Phys.* **2005**, *5*, 053-1123.

(8) Tu P.; Johnston, M. V. Particle Size Dependence of Biogenic Secondary Organic Aerosol Molecular Composition. *Atmos. Chem. Phys.* **2017**, *17*, 7593-7603.

(9) Seinfeld, J. H.; Pandis, S. N. Atmospheric Chemistry and Physics*:* From Air Pollution to Climate Change. John Wiley & Sons, 2016.

(10) Odum, J. R.; Hoffmann, T.; Bowman, F.; Collins, D.; Flagan, R. C.; Seinfeld, J. H. Gas/Particle Partitioning and Secondary Organic Aerosol Yields. *Environ. Sci. Tech.* **1996**, *30*, 2580-2585.

(11) Robinson, A. L.; Donahue, N. M.; Shrivastava, M. K.; Weitkamp, E. A.; Sage, A. M.; Grieshop, A. P.; Lane, T. E.; Pierce, J. R.; Pandis, S. N. Rethinking Organic Aerosols: Semivolatile Emissions and Photochemical Aging. *Science* **2007**, *315*, 1259-1262.

(12) Lim, H. -J.; Turpin, B. J. Origins of Primary and Secondary Organic Aerosol in Atlanta: Results of Time-Resolved Measurements during the Atlanta Supersite Experiment. *Environ. Sci. Technol.* **2002**, *36*, 4489-4496.

(13) Zhao, Z.; Xu, Q.; Yang, X.; Zhang, H. Heterogeneous Ozonolysis of Endocyclic Unsaturated Organic Aerosol Proxies: Implications for Criegee Intermediate Dynamics and Later-generation Reactions, *ACS Earth Space Chem.* **2019**, *33*, 344-356.

(14) Li, Y. J.; Lee, A. K. Y.; Lau, A. P. S.; Chan, C. K. Accretion Reactions of Octanal Catalyzed by Sulfuric Acid: Product Identification, Reaction Pathways, and Atmospheric Implications. *Environ. Sci. Tech.* **2008**, *42*, 7138-7145.

(15) Turpin, B. J.; Saxena, P.; Andrews, E. Measuring and Simulating Particulate Organics in the Atmosphere: Problems and Prospects. *Atmos. Environ.* **2000**, *34*, 2983–3013.

(16) Barsanti, K. C.; Pankow, J. F. Thermodynamics of the Formation of Atmospheric Organic Particulate Matter by Accretion Reactions—2. Dialdehydes, Methylglyoxal, and Diketones. *Atmos. Environ.* **2005**, *39*, 6597–6607.

(17) Djikaev Y. S.; Ruckenstein, E. Effect of Heterogeneous Chemical Reactions on the Köhler Activation of Aqueous Organic Aerosols. *J. Phys. Chem. A* **2018**, *122*, 4322−4337.

(18) Lim, Y. B.; Tan, Y.; Perri, M. J.; Seitzinger, S. P.; Turpin, B. J. Aqueous Chemistry and its Role in Secondary Organic Aerosol (SOA) Formation. *Atmos. Chem. Phys.* **2010**, *10*, 10521-10539.

(19) Rudich, Y.; Donahue, N. M.; Mentel, T. F. Aging of Organic Aerosol: Bridging the Gap between Laboratory and Field Studies. *Ann. Rev. Phys. Chem.* **2007**, *58*, 321–352.

(20) Tobias, H. J.; Ziemann, P. J. Thermal Desorption Mass Spectrometric Analysis of Organic Aerosol Formed from Reactions of 1-Tetradecene and O_3 in the Presence of Alcohols and Carboxylic Acids. *Environ. Sci. Tech.* **2000**, *34*, 2105–2115.

(21) Jang, M.; Kamens, R. M. Atmospheric Secondary Aerosol Formation by Heterogeneous Reactions of Aldehydes in the Presence of a Sulfuric acid Aerosol Catalyst. *Environ. Sci. Tech.* **2001**, *35*, 4758–4766.

(22) Barsanti, K. C.; Pankow, J. F. Thermodynamics of the Formation of Atmospheric Organic Particulate Matter by Accretion Reactions—Part 1: Aldehydes and Ketones. *Atmos. Environ.* **2004**, *38*, 4371–4382.

(23) Johnson, D.; Jenkin, M. E.; Wirtz, K.; Martin-Reviejo, M. Simulating the Formation of Secondary Organic Aerosol from the Photooxidation of Aromatic Hydrocarbons. *Environ. Chem.* **2005**, *2*, 35–48.

(24) Kroll, J. H.; Seinfeld, J. H. Chemistry of Secondary Organic Aerosol: Formation and Evolution of Low-Volatility Organics in the Atmosphere. *Atmos. Environ.* **2008**, *42*, 3593-3624.

(25) Casale, M. T.; Richman, A. R.; Elrod, M. J.; Garland, R. M.; Beaver, M. R.; Tolbert, M. A. Kinetics of Acid-Catalyzed Aldol Condensation Reactions of Aliphatic Aldehydes. *Atmos. Environ.* **2007**, *41*, 6212–6224

(26) Valiev, R. R.; Hasan, G.; Salo, V. -T.; Kubecka, J.; Kurten. T. Intersystem Crossings Drive Atmospheric Gas-Phase Dimer Formation. *J. Phys. Chem. A* **2019**, *123*, 6596-6604.

(27) Louie, M. K.; Francisco, J. S.; Verdicchio, M.; Klippenstein, S. J.; Sinha, A. Dimethylamine Addition to Formaldehyde Catalyzed by a Single Water Molecule: A Facile Route for Atmospheric Carbinolamine Formation and Potential Promoter of Aerosol Growth. *J. Phys. Chem. A* **2016**, *120*, 1358−1368.

(28) Patil, M. P.; Sunoj, R. B. Insights on Co-Catalyst-Promoted Enamine Formation between Dimethylamine and Propanal through Ab Initio and Density Functional Theory Study. *J. Org. Chem.* **2007**, *72*, 8202−8215.

(29) Sayer, J. M.; Jencks, W. P. Mechanism and Catalysis of 2-methyl-3-thiosemicarbazone Formation. Second Change in Rate determining Step and Evidence for a Stepwise Mechanism for Proton Transfer in a Simple Carbonyl Addition Reaction. *J. Am. Chem. Soc.* **1973**, *95*, 5637−5649.

(30) Duporté, G.; Riva, M.; Parshintsev, J.; Heikkinen, E.; Barreira, L. M.; Myllys, N.; Heikkinen, L.; Hartonen, K. M.; Kulmala, M.; Ehn, M., et al. Chemical Characterization of Gas- and Particle-Phase Products from the Ozonolysis of α-Pinene in the Presence of Dimethylamine. *Environ. Sci. Technol.* **2017**, *51*, 5602−5610.

(31) Hirvonen, V.; Myllys, N.; Kurtén, T.; Elm, J. Closed-Shell Organic Compounds Might Form Dimers at the Surface of Molecular Clusters. *J. Phys. Chem. A* **2018**, *122*, 1771-1780.

(32) Liu, C.; Chu, B.; Liu, Y.; Ma, Q.; Ma, J.; He, H.; Li, J.; Hao, J. Effect of Mineral Dust on Secondary Organic Aerosol Yield and Aerosol Size in α-pinene/NOx Photo-Oxidation. *Atmos. Environ.* **2013**, *77*, 781-789.

(33) Usher, C. R.; Michel, A. E.; Stec, D.; Grassian, V. H. Laboratory Studies of Ozone Uptake on Processed Mineral Dust. *Atmos. Environ.* **2003**, *37*, 5337-5347.

(34) Cocker, D. R.; Mader, B. T.; Kalberer, M.; Flagan, R. C.; Seinfeld, J. H. The Effect of Water on Gas–Particle Partitioning of Secondary Organic Aerosol: II. m-Xylene and 1, 3, 5-Trimethylbenzene Photooxidation Systems. *Atmos. Environ.* **2001**, *35*, 6073-6085.

(35) Jang, M. S.; Kamens, R. M. Characterization of Secondary Aerosol from the Photooxidation of Toluene in the Presence of NOx and 1-Propene. *Environ. Sci. Technol.* **2001**, *35*, 3626-3639.

(36) Forstner, H. J. L.; Flagan, R. C.; Seinfeld, J. H. Secondary Organic Aerosol from the Photooxidation of Aromatic Hydrocarbons: Molecular Composition. *Environ. Sci. Technol.* **1997**, *31*, 1345-1358.

(37) Frisch, M. J.; Trucks, G. W.; Schlegel, H. B.; Scuseria, G. E.; Robb, M. A.; Cheeseman, J. R.; Scalmani, G.; Barone, V.; Petersson, G. A.; Nakatsuji, H., et al. Gaussian, Inc.; Wallingford CT, 2016.

(38) Chai, J. D.; Head-Gordon, M. Long-range Corrected Hybrid Density Functionals with Damped Atom–Atom Dispersion Corrections. *Phys. Chem. Chem. Phys.* **2008**, *10*, 6615-6620.

(39) Chen, W. L.; Hsieh, C. M.; Yang, L.; Hsu, C. C.; Lin, S. T. A Critical Evaluation on the Performance of COSMO-SAC Models for Vapor–Liquid and Liquid–Liquid Equilibrium Predictions Based on Different Quantum Chemical Calculations. *Ind. Eng. Chem. Res.* **2016**, *55*, 9312-9322.

(40) Singh, D. K.; Rathke, B.; Kiefer, J.; Materny, A. Molecular Structure and Interactions in the Ionic Liquid 1-Ethyl-3-methylimidazolium Trifluoromethanesulfonate. *J. Phys. Chem. A* **2016**, *120*, 6274-6286.

(41) Riplinger, C.; Neese, F. An Efficient and Near Linear Scaling Pair Natural Orbital Based Local Coupled Cluster Method. *J. Chem. Phys.* **2013**, *138*, 034106-034118.

(42) Riplinger, C.; Sandhoefer, B.; Hansen, A.; Neese, F. Natural Triple Excitations in Local Coupled Cluster Calculations with Pair Natural Orbitals. *J. Chem. Phys.* **2013**, *139*, 134101-134113.

(43) Riplinger, C.; Pinski, P.; Becker, U.; Valeev, E. F.; Neese, F. Sparse Maps - A Systematic Infrastructure for Reduced-scaling Electronic Structure Methods. II. Linear Scaling Domain Based Pair Natural Orbital Coupled Cluster Theory. *J. Chem. Phys.* **2016**, *144*, 024109-024120.

(44) Eugene, P.; Kazakov, A. Efficient DLPNO–CCSD (T)-based Estimation of Formation Enthalpies for C-, H-, O-, and N-Containing Closed-Shell Compounds Validated Against Critically Evaluated Experimental Data. *J. Phys. Chem. A* **2017**, *121*, 4379-4387.

(45) Werner, H. –J.; Adler, T. B.; Manby, F. R. General Orbital Invariant MP2-F12 Theory. *J. Chem. Phys.* **2007**, *126*, 164102-164118.

(46) Dunning, T. H. Gaussian Basis Sets for use in Correlated Molecular Calculations. I. The Atoms Boron through Neon and Hydrogen. *J. Chem. Phys.* **1989**, *90*, 1007−1023.

(47) Kendall, R. A.; Dunning, T. H.; Harrison, R. J. Electron Affinities of the Firstrow Atoms Revisited. Systematic Basis Sets and Wave Functions. *J. Chem. Phys.* **1992**, *96*, 6796−6806.

(48) Neese, F. The ORCA Program System. *Wiley Interdiscip. Rev. Comput. Mol. Sci.* **2012**, *2*, 73−78.

(49) Jensen, F. *Introduction to Computational Chemistry*; John wiley & sons, 2017.

(50) Vereecken, L.; Francisco, J. S. Theoretical Studies of Atmospheric Reaction Mechanisms in the Troposphere. *Chem. Soc. Rev.* **2012**, *41*, 6259-6293.

(51) Fukui, K. The Path of Chemical-Reactions – The IRC Approach. *Acc. Chem. Res.* **1981**, *14*, 363-368.

(52) Hratchian, H. P.; Schlegel, H. B. Theory and Applications of Computational Chemistry: The First 40 Years, Elsevier, Amsterdam, 2005, 195-249.

(53) Zhang, J.; Dolg, M.; ABCluster: The Artificial Bee Colony Algorithm for Cluster Global Optimization. *Phys. Chem. Chem. Phys.* **2015**, *17*, 24173-24181.

(54) Zhang, J.; Dolg, M.; Global Optimization of Clusters of Rigid Molecules by the Artificial Bee Colony Algorithm. *Phys. Chem. Chem. Phys.* **2016**, *18*, 3003-3010.

(55) Bannwarth, C.; Ehlert, S.; Grimme, S. GFN2-xTB—An Accurate and Broadly Parametrized Self-Consistent Tight-Binding Quantum Chemical Method with Multipole Electrostatics and Density-Dependent Dispersion Contributions. *J. Chem. Theory Comput.* **2018**, *15*, 1652-1671.

(56) Grimme, S.; Bannwarth, C.; Shushkov, P. A Robust and Accurate Tight-Binding Quantum Chemical Method for Structures, Vibrational Frequencies, and Noncovalent Interactions of Large Molecular Systems Parametrized for All spd-Block Elements (Z= 1–86). *J. Comput. Theory Chem.* **2017**, *13*, 1989-2009.

(57) Matsuki, A.; Schwarzenboeck, A.; Venzac, H.; Laj, P.; Crumeyrolle, S.; Gomes, L. Cloud Processing of Mineral Dust: Direct Comparison of Cloud Residual and Clear Sky Particles during AMMA Aircraft Campaign in Summer 2006. *Atmos. Chem. Phys.* **2010**, *10*, 1057-1069.

(58) Pöschl, U. Atmospheric Aerosols: Composition, Transformation, Climate and Health Effects. *Angew. Chem.* **2005**, *44*, 7520-7540.

(59) Li, W. J.; Shao, L. Y. Observation of Nitrate Coatings on Atmospheric Mineral Dust Particles. *Atmos. Chem. Phys.* **2009**, *9*, 1863-1871.

(60) Marsden, N. A.; Ullrich, R.; Möhler, O.; Eriksen Hammer, S.; Kandler, K.; Cui, Z.; Williams, P. I.; Flynn, M. J.; Liu, D.; Allan, J. D., et al. Mineralogy and Mixing State of North African Mineral Dust by On-Line Single-Particle Mass Spectrometry. *Atmos. Chem. Phys. Discuss.* **2018**, *19*, 2259-2281.

(61) Claquin, T.; Schulz, M.; Balkanski, Y. J. Modeling the Mineralogy of Atmospheric Dust Sources. *J. Geophys. Res. Atmos.* **1999**, *104*, 22243-22256.

(62) Ji, Y.; Wang, H.; Li, G.; An, T. Theoretical Investigation on the Role of Mineral Dust Aerosol in Atmospheric Reaction: A Case of the Heterogeneous Reaction of Formaldehyde with NO_2 onto SiO_2 Dust Surface. *Atmos. Environ.* **2015**, *103*, 207-214.

(63) Moreno, T.; Querol, X.; Castillo, S.; Alastuey, A.; Cuevas, E.; Herrmann, L.; Mounkaila, M.; Elvira, J.; Gibbons, W. Geochemical Variations in Aeolian Mineral Particles from the Sahara–Sahel Dust Corridor. *Chemosphere* **2006**, *65*, 261-270.

(64) Lindberg, J. D. The Composition and Optical Absorption Coefficient of Atmospheric Particulate Matter. *Opt. Quant. Electron.* **1975**, *7*, 131-139.

(65) Krueger, B. J.; Grassian, V. H.; Cowin, J. P.; Laskin, A. Heterogeneous Chemistry of Individual Mineral Dust Particles from Different Dust Source Regions: The Importance of Particle Mineralogy. *Atmos. Environ.* **2004**, *38*, 6253-6261.

(66) Adushkin, V. V., Chen, B. B., Popel, S. I., Dubinskii, A. Y., Weidler, P. G.; Friedrich, F. Experimental Study of Small-Scale Mineral Particles in the Atmosphere of Central Asia. *Izv. Phys. Solid Earth* **2018**, *54*, 330-335.

(67) Zeb, B.; Alam, K.; Sorooshian, A.; Blaschke, T.; Ahmad, I.; Shahid, I. On the Morphology and Composition of Particulate Matter in an Urban Environment. *Aerosol Air Qual. Res.* **2018**, *18*, 1431-1447.

(68) Kandler, K.; Schütz, L.; Deutscher, C.; Ebert, M.; Hofmann, H.; Jäckel, S.; Jaenicke, R.; Knippertz, P.; Lieke, K.; Massling, A., et al. A. Size Distribution, Mass Concentration, Chemical and Mineralogical Composition and Derived Optical Parameters of the Boundary Layer Aerosol at Tinfou, Morocco, during SAMUM 2006. *Tellus B Chem. Phys. Meteor.* **2009**, *61*, 32-50.

(69) Kumar, A.; Marcolli, C.; Luo, B.; Peter, T. Ice Nucleation Activity of Silicates and Aluminosilicates in Pure Water and Aqueous Solutions–Part 1: The K-Feldspar Microcline. *Atmos. Chem. Phys.* **2018**, *18*, 7057-7079.

(70) Ryder, C. L.; Marenco, F.; Brooke, J. K.; Estelles, V.; Cotton, R.; Formenti, P.; McQuaid, J. B.; Price, H. C.; Liu, D.; Ausset, P.; Rosenberg, P. D. Coarse-Mode Mineral Dust Size Distributions, Composition and Optical Properties from AER-D Aircraft Measurements over the Tropical Eastern Atlantic. *Atmos. Chem. Phys.* **2018**, *18*, 17225-17257.

(71) Civalleri, B.; Garrone, E.; Ugliengo, P. Vibrational Modes of Isolated Hydroxyls of Silica Computed Ab Initio in a Cluster Approach. *Chem. Phys. Lett.* **1998**, *294*, 103-108.

(72) Iuga, C.; Vivier-Bunge, A.; Hernandez-Laguna, A.; Sainz-Diaz, C. I. Quantum Chemistry and Computational Kinetics of the Reaction between OH Radicals and Formaldehyde Adsorbed on Small Silica Aerosol Models. *J. Phys. Chem. C* **2008**, *112*, 4590-4600.

(73) Pereira, J. C. G.; Catlow, C. R. A.; Price, G. D. Ab Initio Studies of Silica-Based Clusters. Part II. Structures and Energies of Complex Clusters. *J. Phys. Chem. A* **1999**, *103*, 3268-3284.

(74) Hermans, I.; Vereecken, L.; Jacobs, P. A.; Peeters, J. Mechanism of the Catalytic Oxidation of Hydrocarbons by N-hydroxyphthalimide: A Theoretical Study. *Chem. Comm.* **2004**, *9*, 1140-1141.

(75) Eckart, C. The Penetration of a Potential Barrier by Electrons. *Phys. Rev.* **1930**, *35*, 1303-1309.

(76) Sarkar, S.; Mallick, S.; Kumar, P.; Bandyopadhyay, B. Isomerization of Methoxy Radical in the Troposphere: Competition between Acidic, Neutral and Basic Catalysts. *Phys. Chem. Chem. Phys.* **2017**, *19*, 27848-27858.

(77) Wehner, B.; Wiedensohler, A.; Tuch, T. M.; Wu, Z. J.; Hu, M.; Slanina, J.; Kiang, C. S. Variability of the Aerosol Number Size Distribution in Beijing, China: New Particle Formation, Dust Storms, and High Continental Background. *Geophys. Res. Lett.* **2004**, *31*, L22108- L22111.

(78) Möhler, O.; Field, P. R.; Connolly, P.; Benz, S.; Saathoff, H.; Schnaiter, M.; Wagner, R.; Cotton, R.; Krämer, M.; Mangold, A.; Heymsfield, A. J. Efficiency of the Deposition Mode Ice Nucleation on Mineral Dust Particles. *Atmos. Chem. Phys.* **2006**, *6*, 3007-3021.

(79) Karagulian, F.; Santschi, C.; Rossi, M. J. The Heterogeneous Chemical Kinetics of N_2O_5 on $CaCO_3$ and Other Atmospheric Mineral Dust Surrogates. *Atmos. Chem. Phys.* **2006**, *6*, 1373-1388.

(80) Gao, Z.; Wang, X.; Shen, L.; Xiang, H.; Wang, H. Characteristics of Aerosol Chemical Compositions and Size Distributions during a Long-Range Dust Transport Episode in an Urban City in the Yangtze River Delta. *Atmosphere* **2019**, *10*, 68-82.
(81) Chemcraft-Graphical Software for Visualization of Quantum Chemistry Computations. https://www.chemcraftprog.com
(82) Sipilä, M.; Berndt, T.; Petäjä, T.; Brus, D.; Vanhanen, J.; Stratmann, F.; Patokoski, J.; Mauldin, R. L.; Hyvärinen, A. P.; Lihavainen, H., et al. The Role of Sulfuric Acid in Atmospheric Nucleation. *Science* **2010**, *327*, 1243-1246.

TOC Graphic

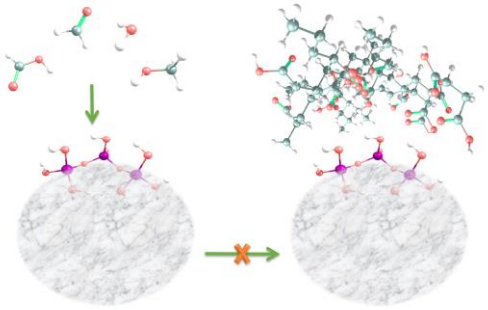

Supporting Information

Computational Study of the Effect of Mineral Dust on Secondary Organic Aerosol Formation by Accretion Reactions of Closed-Shell Organic Compounds

Fatemeh Keshavarz*[,a], Anna Shcherbacheva[a], Jakub Kubečka[a], Hanna Vehkamäki[a], Theo Kurtén[b]

a) Institute for Atmospheric and Earth System Research, Faculty of Science, University of Helsinki, FI-00014, Finland
b) Department of Chemistry, Faculty of Science, University of Helsinki, FI-00014, Finland

* Corresponding author: Fatemeh Keshavarz: fatemeh.keshavarz@helsinki.fi

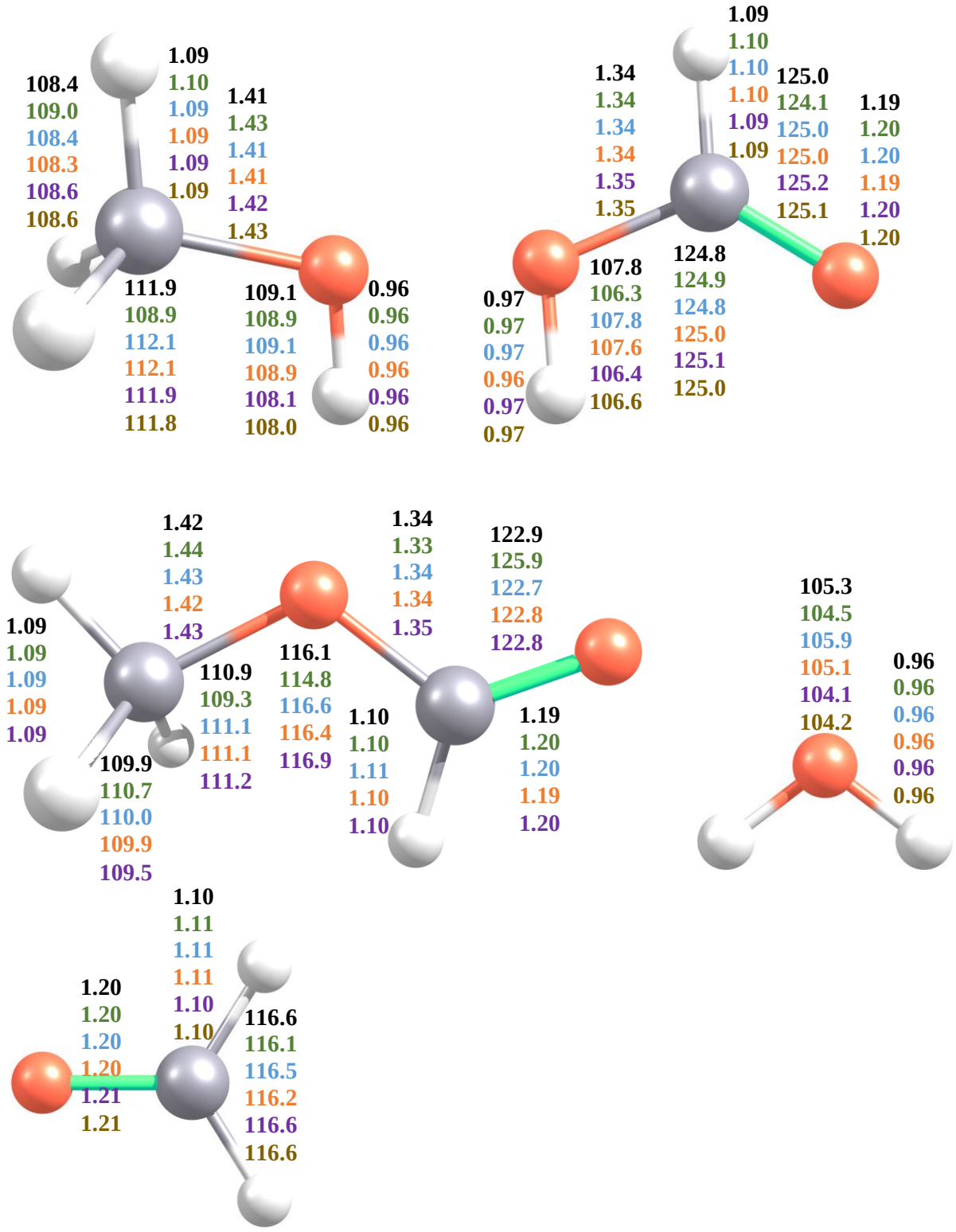

Figure S1. Geometries of the reactants and products at the M06-2X/aug-cc-pVTZ (black), ωB97X-D/6-31++G** (blue), ωB97X-D/aug-cc-pVTZ (orange), MP2/aug-cc-pVTZ (purple) and CCSD(T)/aug-cc-pVTZ (dark yellow) levels of theory as compared with the experimentally determined structures (green: CH_3OH[1], syn-$HCOOH$[2], CH_3CHO[3], H_2O[4] and CH_2O[5]).

Table S1. Reaction Enthalpy at Different Levels of Theory as Compared with Experimental Data, at 0 K

Products	CH_3OH+syn-HCOOH to $CH_3OCHO+H_2O$	syn-HCOOH to anti-HCOOH	CH_2O+H_2O to $CH_2(OH)_2$	MAE* (%)
ATcT**	-19.0	16.4	-34.9	-
ωB97X-D/6-31++G**	-17.1	20.0	-47.5	22.68
CCSD(T)/aug-cc-pVTZ//wB97X-D/6-311++G**	-20.8	16.7	-34.1	4.50
MPWB1K/aug-cc-pVTZ	-16.8	17.1	-49.4	19.15
wB97X-D/aug-cc-pVTZ	-17.2	16.4	-39.5	7.53
CBS-QB3	-26.2	15.7	-9.3	38.47
M06-2X/aug-cc-pVTZ	-18.5	17.5	-50.1	17.64
MP2/aug-cc-pVTZ	-22.5	16.8	-34.5	7.33
CCSD(T)/aug-cc-pVTZ	NA***	16.6	NA	-
CCSD(T)/aug-cc-pVTZ//M06-2X/aug-cc-pVTZ	-21.0	16.8	-35.1	4.54
DLPNO-CCSD(T)/aug-cc-pVTZ// ωB97X-D/6-31++G**	-21.0	16.8	-34.1	5.05
M06-2X/6-311++G**	-17.9	19.6	-49.2	22.06

***** Mean Absolute Error

** Active Thermochemical Tables (version 1.122d); https://atct.anl.gov/

*** Not available

Table S2. Comparison of the Geometry of the Mono- and Tri-Silicic acid Models Optimized at the ωB97X-D/6-31++G** Level of Theory with the Experimentally Resolved SiO_2 Units' of Quartz, K-Feldspar and Kaolinite, as the Materials Representing Dust Particles

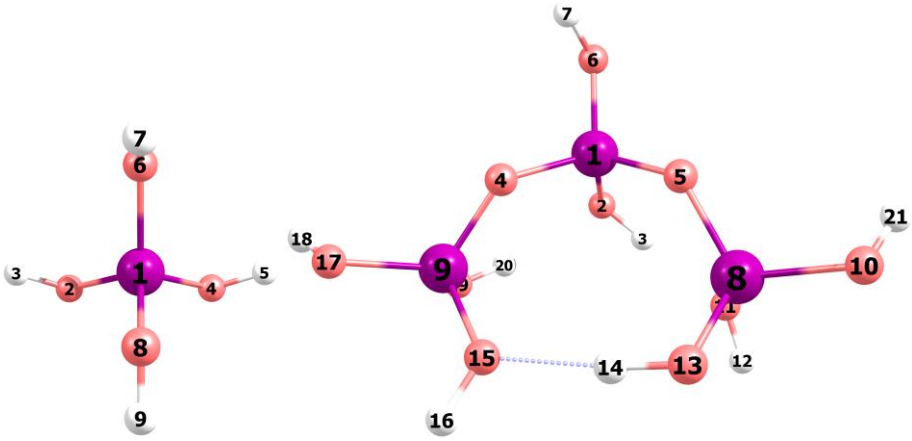

Structure	O6-H7 (Å)	Si1-O6 (Å)	H7-O6-Si1 (°)	H5-O4-Si1 (°)	O2-Si1-O4 (Mcat.) O4-Si1-O5 (Tcat.) (°)	O6-Si1-O2 (Mcat.) O6-Si1-O4 (Tcat.) (°)
ωB97X-D/6-31++G** (Mcat.)	0.96	1.64	116.1	117.4	102.8	112.5
ωB97X-D/6-31++G** (Tcat.)	0.96	1.63	117.8	-	109.1	109.5
Quartz[6]	-	1.60	-	-	89.4	112.5
Quartz[7]	-	1.58	-	-	109.7	109.9
Quartz[8]	-	1.59	-	-	107.4	110.1
K-Feldspar[9]	-	1.65	-	-	109.0	111.6
Orthoclase Feldspar[10]	-	1.62	-	-	109.5	112.0
Monoclinic K-feldspar[11]	-	1.64	-	-	104.4	111.8
Kaolinite[12]	-	1.60	-	-	106.6	111.6
Kaolinite[13]	-	1.61	-	-	106.4	111.6

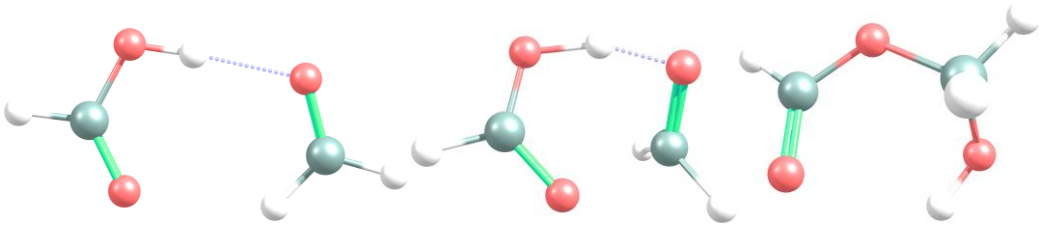

RC-FFA **TS-FFA** **HCO_2CH_2OH**

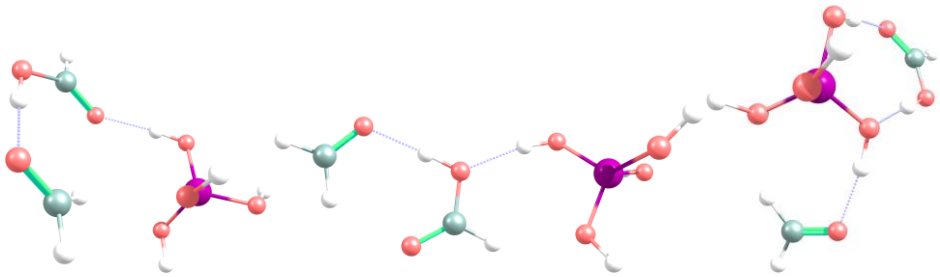

RC1(M)-FFA **RC2(M)-FFA** **RC3(M)-FFA**

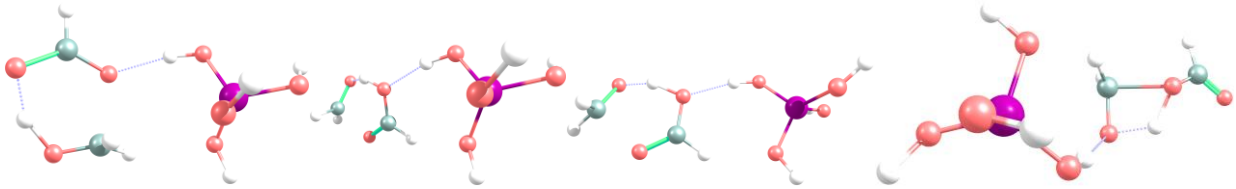

TSM1-FFA **TSM2-FFA** **TSM2-FFA** **TSM3-FFA**

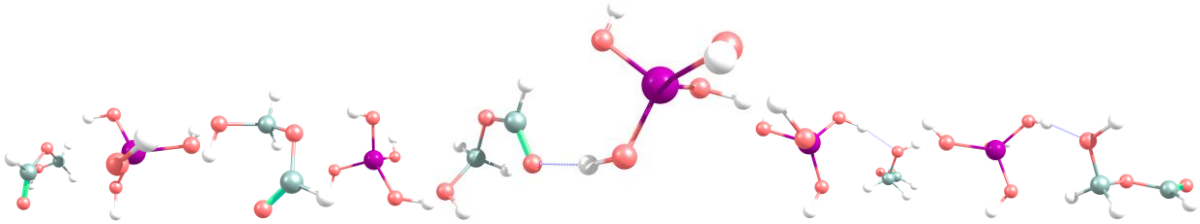

PC1(M)-FFA **PC1(M)-FFA** **PC2(M)-FFA** **PC3(M)-FFA** **PC3(M)-FFA**

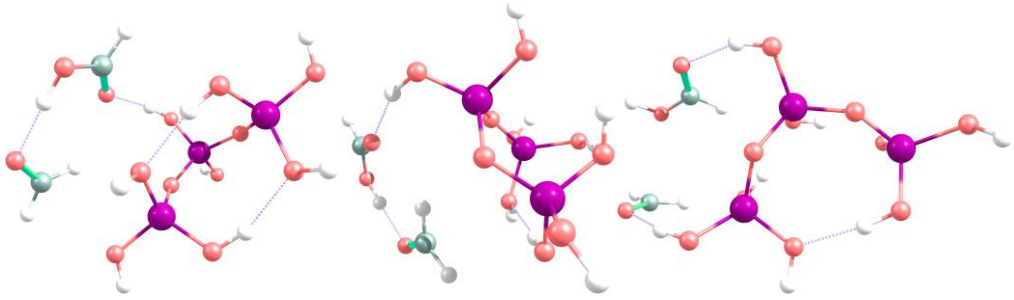

RC1(T)-FFA **RC2(T)-FFA** **RC3(T)-FFA**

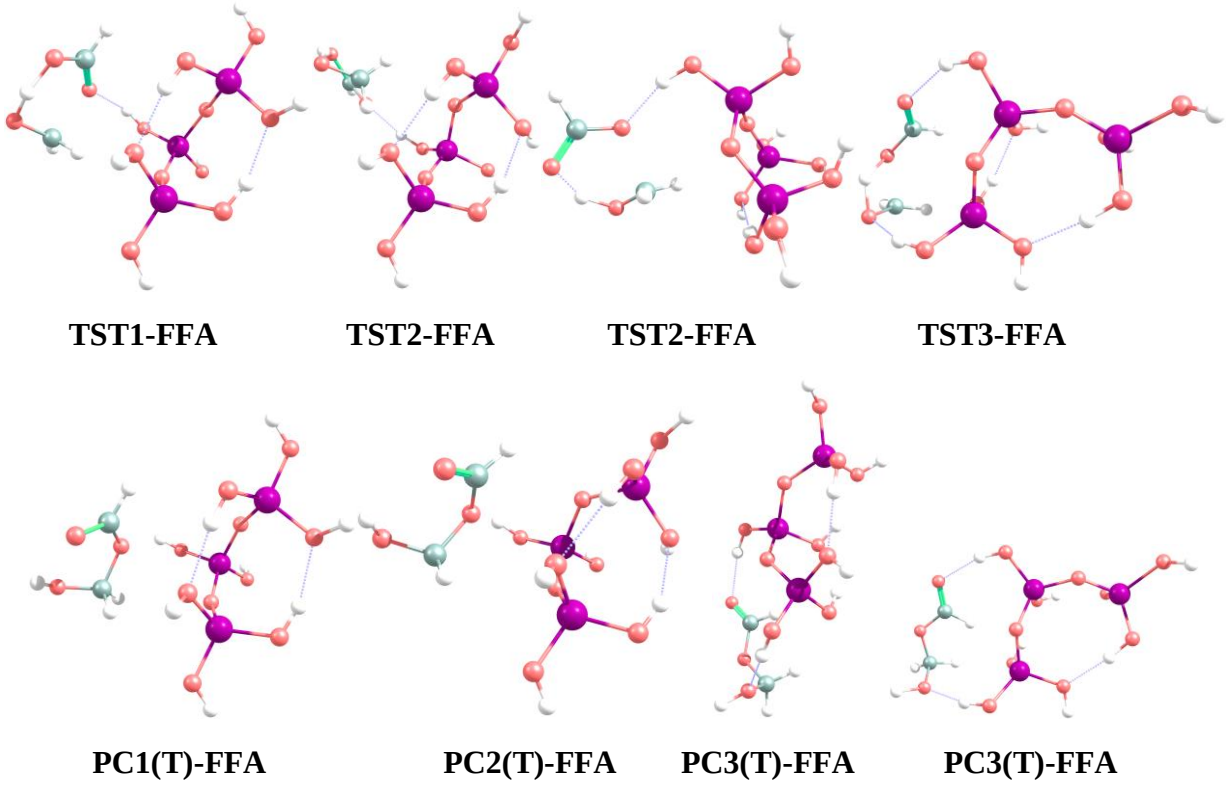

Figure S2. Geometries of the species involved in R7. The blue dotted lines represent H-bonding.

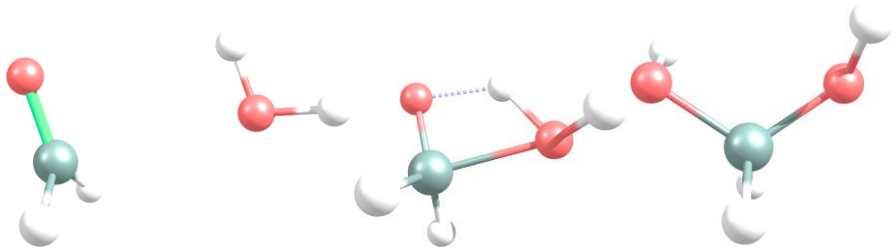

RC-FW **TS-FW** **$CH_2(OH)_2$**

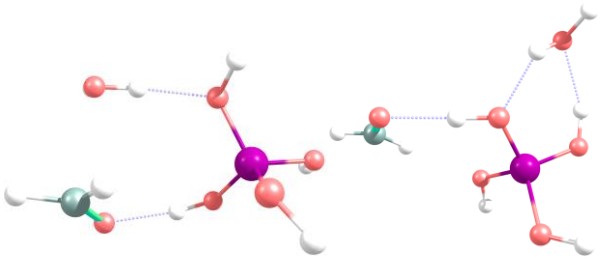

RC1(M)-FW **RC2(M)-FW**

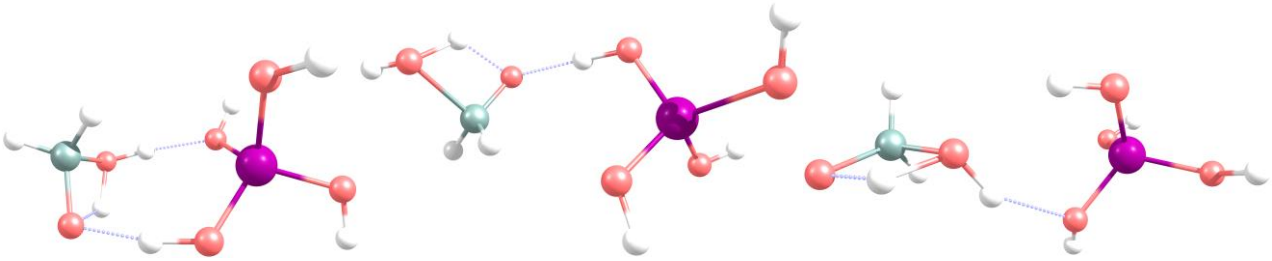

TSM1-FW **TSM2-FW** **TSM3-FW**

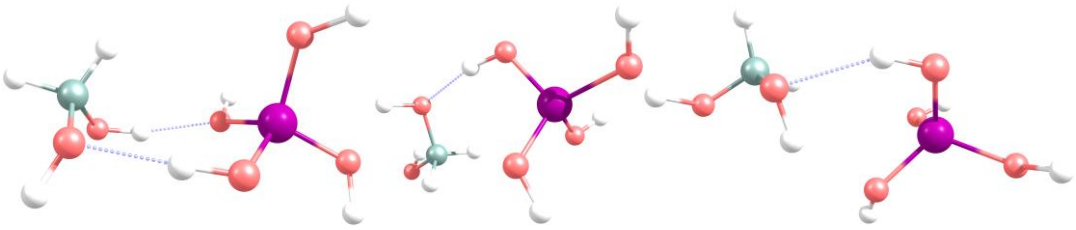

PC1(M)-FW **PC2(M)-FW** **PC3(M)-FW**

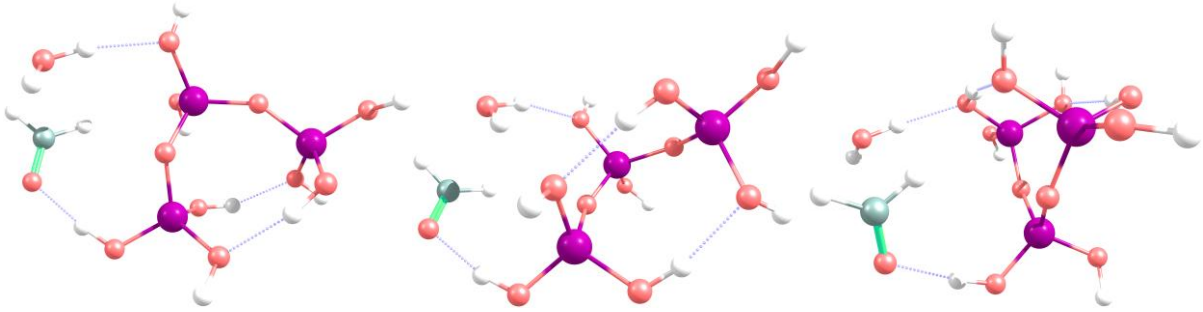

RC1(T)-FW **RC2(T)-FW** **RC3(T)-FW**

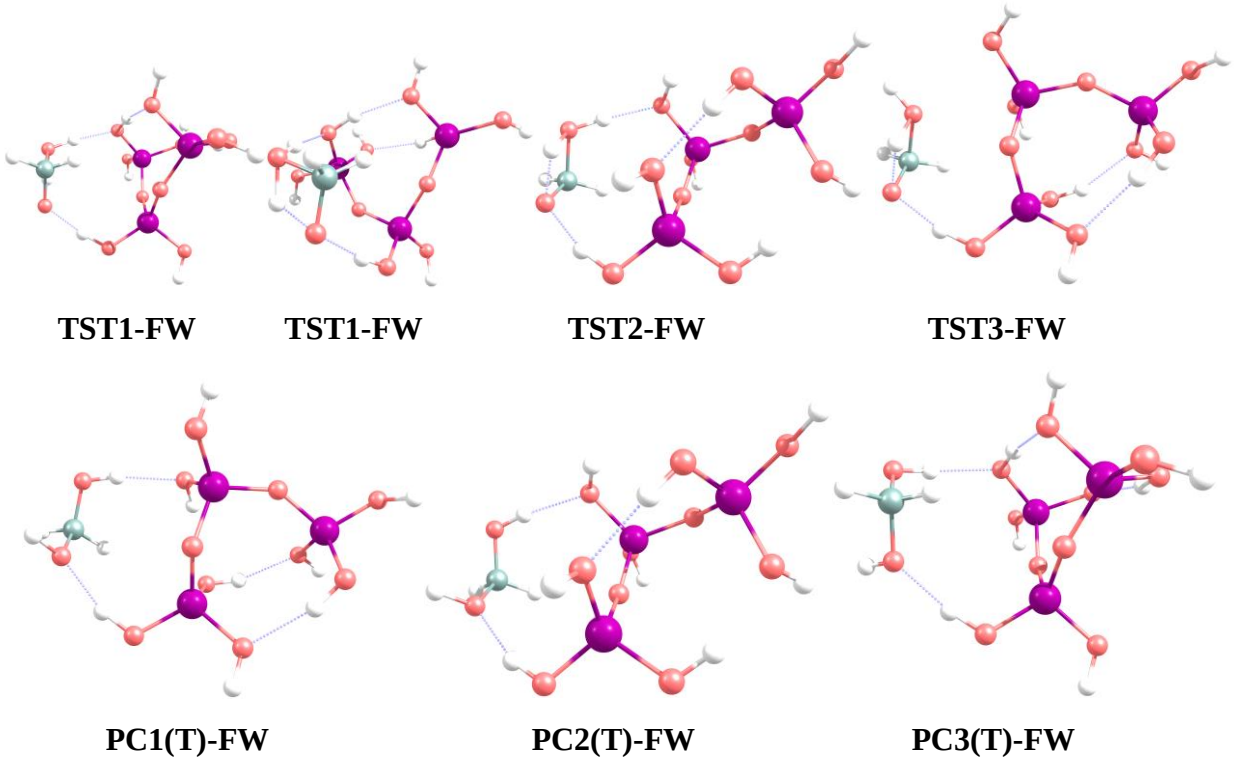

Figure S3. Geometries of the species involved in R8. The blue dotted lines represent H-bonding.

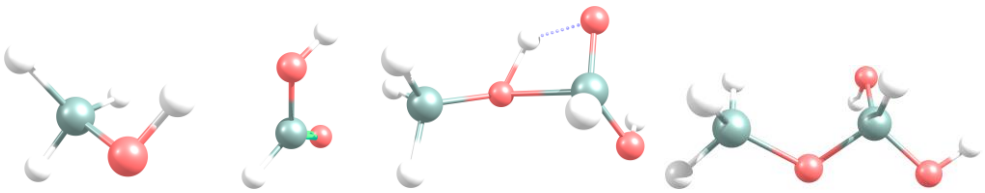

RC-FAM **TS1-FAM** **INT**

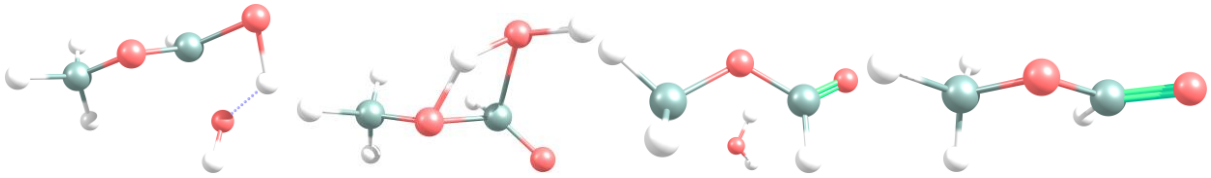

TS2-FAM **TS3-FAM** **PC-FAM** **CH_3OCHO**

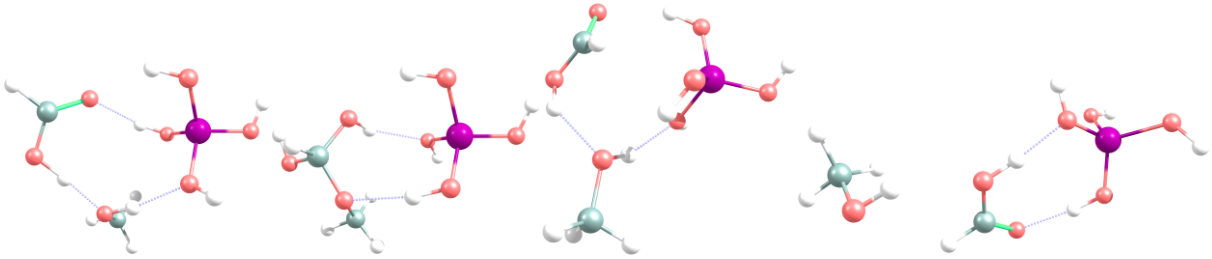

RC1(M)-FAM **INTM** **RC2(M)-FAM** **RC3(M)-FAM**

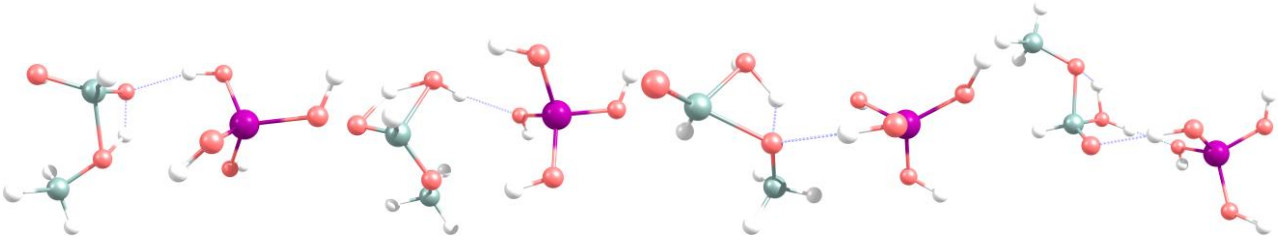

TSM1-FAM **TSM2-FAM** **TSM3-FAM** **TSM4-FAM**

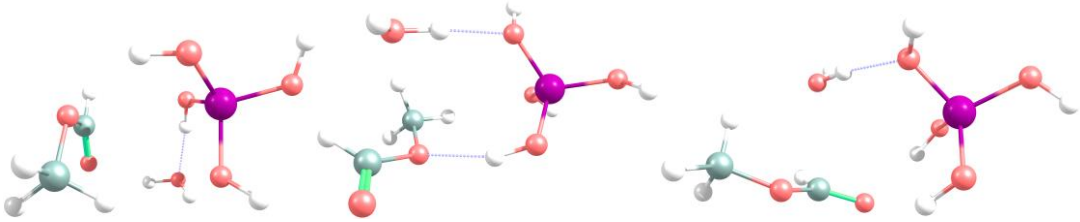

PC1(M)-FAM **PC2(M)-FAM** **PC3(M)-FAM**

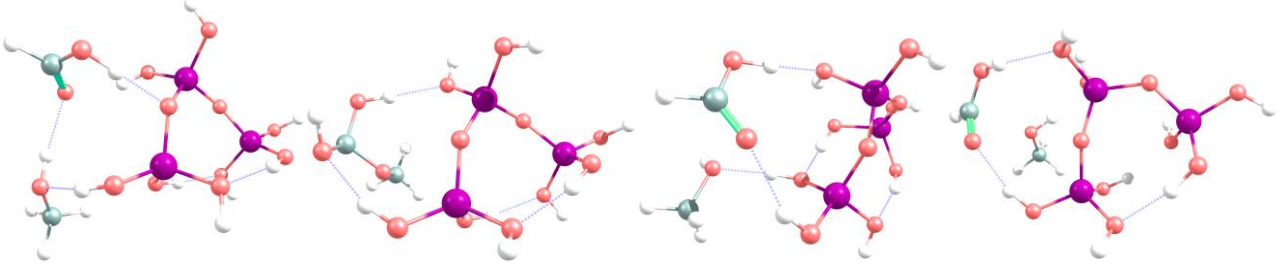

RC1(T)-FAM **INTT** **RC2(T)-FAM** **RC3(T)-FAM**

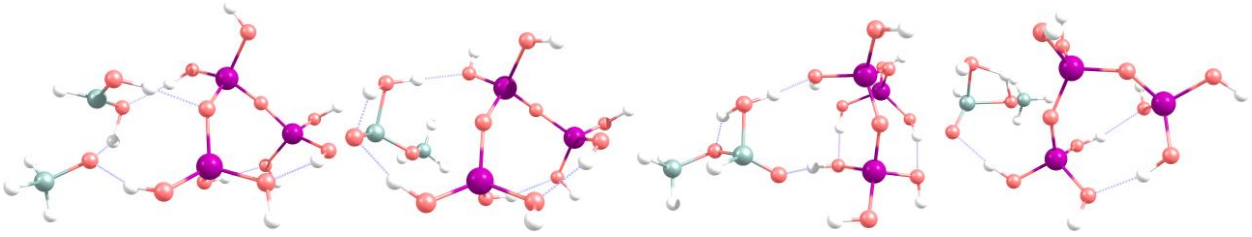

TST1-FAM **TST2-FAM** **TST3-FAM** **TST4-FAM**

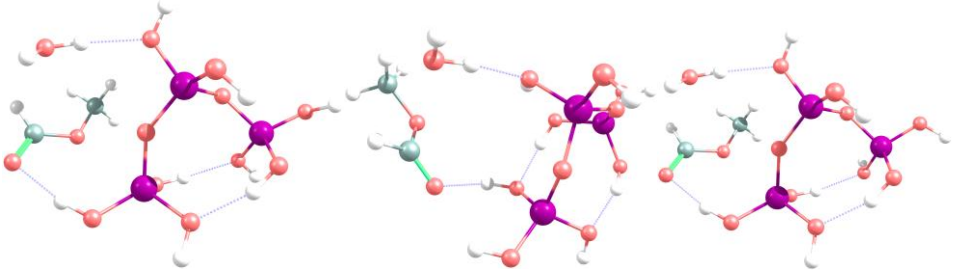

PC1(T)-FAM **PC2(T)-FAM** **PC3(T)-FAM**

Figure S4. Geometries of the species involved in R9. The blue dotted lines represent H-bonding.

Table S3. The Gibbs Free Energy Values of the Pre- and Post-Reaction Complexes Relative to the Reactants in kJ mol^{-1}, at 1 atm

	298 K	198 K		298 K	198 K
			R7		
RC1(M)-FFA	-3.7	-33.4	PC1(M)-FFA	-1.1	-34.2
RC2(M)-FFA	2.2	-25.9	PC2(M)-FFA	-11.9	-44.0
RC3(M)-FFA	-19.2	-49.0	PC3(M)-FFA	16.2	-14.2
RC-FFA	-10.9	-24.8	PC1(T)-FFA	-12.5	-43.9
RC1(T)-FFA	-9.7	-40.1	PC2(T)-FFA	-6.3	-39.9
RC2(T)-FFA	-7.1	-37.8	PC3(T)-FFA	-4.7	-38.8
RC3(T)-FFA	8.0	-22.2			
			R8		
RC1(M)-FW	26.9	-1.4	PC1(M)-FW	1.3	-30.1
RC2(M)-FW	17.7	-10.2	PC2(M)-FW	-0.1	-27.9
RC-FW	17.2	8.7	PC3(M)-FW	11.4	-18.8
RC1(T)-FW	22.8	-4.9	PC1(T)-FW	3.4	-27.4
RC2(T)-FW	152.6	123.3	PC2(T)-FW	9.0	-22.3
RC3(T)-FW	22.0	-5.6	PC3(T)-FW	-2.7	-33.2
			R9		
RC1(M)-FAM	25.0	-54.8	PC1(M)-FAM	-10.4	-42.9
RC2(M)-FAM	9.2	-21.8	PC2(M)-FAM	6.8	-23.3
RC3(M)-FAM	-3.8	-31.7	PC3(M)-FAM	-1.8	-32.0
RC-FAM	4.5	-6.5	PC-FAM	-0.2	-11.4
RC1(T)-FAM	-15.3	-46.0	PC1(T)-FAM	-3.3	-33.0
RC2(T)-FAM	-11.7	-43.1	PC2(T)-FAM	-5.6	-35.9
RC3(T)-FAM	3.0	-27.8	PC3(T)-FAM	2.2	-28.7

Table S4. The Imaginary Frequency (υ*; cm^{-1}), $\Delta_r^{\#}G$ (kJ mol^{-1}), $\Delta_r^{\#}H$ (kJ mol^{-1}), $\Delta_r^{\#}S$ (J mol^{-1}) and κ_r Values of the Studied Reaction Paths, at 1 atm

Reaction path	υ*	κ_r (298 K)	κ_r (198 K)	$\Delta_r^{\#}G$ (298 K)	$\Delta_r^{\#}G$ (198 K)	$\Delta_r^{\#}H$ (298 K)	$\Delta_r^{\#}H$ (198 K)	$\Delta_r^{\#}S$ (298 K)	$\Delta_r^{\#}S$ (198 K)
r0 (TS-FFA; R7)	1075.765	2.26	3.74	67.1	49.3	13.8	14.8	-178.8	-115.8
r1 (TSM1-FFA)	1128.974	2.25	3.82	77.8	45.4	-18.7	-18.8	-323.7	-215.3
r2 (TSM2-FFA)	1065.428	1.88	3.16	78.0	45.7	-18.1	-18.0	-322.4	-213.8
r3 (TSM3-FFA)	1717.919	3.33	6.67	204.0	173.1	112.2	111.8	-308.0	-205.8
r1 (TST1-FFA)	1151.572	2.13	3.67	69.9	38.2	-23.9	-24.5	-314.7	-210.4
r2 (TST2-FFA)	1034.359	1.90	3.13	75.6	42.5	-22.9	-23.2	-330.3	-220.4
r3 (TST3-FFA)	1710.352	3.90	7.50	191.8	156.8	87.7	87.6	-349.0	-232.0
r0 (TS-FW; R8)	1696.876	3.82	7.35	191.6	176.4	145.3	147.3	-155.3	-97.7
r1 (TSM1-FW)	1517.524	3.29	6.13	168.2	134.9	67.6	70.0	-337.4	-217.6
r2 (TSM2-FW)	1513.426	3.26	6.07	191.0	160.8	100.1	101.7	-304.7	-198.3
r3 (TSM3-FW)	1679.596	3.78	7.24	197.9	168.2	108.5	110.0	-299.8	-195.4
r1 (TST1-FW)	1502.738	3.26	6.05	157.0	124.3	58.5	60.4	-330.2	-214.2
r2 (TST2-FW)	1491.015	3.21	5.95	168.6	135.1	67.7	69.8	-338.3	-218.9
r3 (TST3-FW)	1525.924	3.30	6.16	197.2	164.4	98.7	100.1	-330.4	-215.5
r0 (TS2-FAM; R9)	1783.048	4.12	8.02	188.8	171.9	138.6	138.7	-168.5	-111.3
r0 (TS3-FAM; R9)	1335.441	2.75	4.93	204.3	187.8	155.4	155.4	-163.9	-108.8
r1 (TSM2-FAM)	1798.032	4.20	8.18	190.7	156.3	88.4	88.2	-343.2	-228.4
r2 (TSM3-FAM)	1283.003	2.61	4.63	231.7	199.8	137.3	136.4	-316.6	-212.8
r3 (TSM4-FAM)	1364.731	2.84	5.13	194.7	161.0	94.3	94.3	-336.6	-223.7
r1 (TST2-FAM)	1649.173	3.71	7.07	172.2	136.4	65.8	65.6	-356.7	-237.5
r2 (TST3-FAM)	1376.308	2.88	5.21	192.5	156.6	85.5	85.8	-358.9	-237.6
r3 (TST4-FAM)	1414.709	2.97	5.43	204.3	170.8	105.1	104.2	-332.7	-223.4

Section S.A. The Cartesian coordinates of the geometries optimized at the ωB97X-D/6-31++G** level.

Mcat

Si	-0.02408	0.00002	-0.01490
O	-1.04470	1.28060	-0.08022
H	-0.65897	2.14416	-0.23593
O	-1.04460	-1.28046	-0.08364
H	-0.65868	-2.14364	-0.24096
O	1.06831	0.00179	-1.24634
H	1.99320	0.00142	-0.99052
O	0.91917	-0.00186	1.34519
H	0.47619	-0.00287	2.19606

Tcat

Si	-0.008980	1.458860	-0.180210
O	0.080940	1.474160	1.466840
H	-0.665430	1.023960	1.892420
O	1.269520	0.588880	-0.744310
O	-1.401410	0.724070	-0.635790
O	0.074890	2.982830	-0.750800
H	0.377300	3.106200	-1.652570
Si	-2.200910	-0.600810	-0.081570
Si	2.179850	-0.584860	-0.055160
O	-3.742610	-0.633640	-0.620210
O	-2.111760	-0.364050	1.572410
H	-2.394120	-1.090250	2.133140
O	-1.537610	-2.012460	-0.529700
H	-0.568680	-2.079140	-0.469160
O	1.257590	-1.961380	-0.179840
H	1.708240	-2.796430	-0.030490
O	3.574020	-0.892540	-0.852100
H	4.346900	-0.390070	-0.585560
O	2.535040	-0.178270	1.492810
H	1.892500	0.417330	1.904280
H	-4.265100	0.162840	-0.509400

CH_2O

C	0.52978	0.00000	0.00000
O	-0.67543	0.00000	0.00000
H	1.11234	0.94104	0.00001
H	1.11239	-0.94101	0.00001

syn-HCO_2H

C	0.13126	0.40136	0.00000
O	1.13344	-0.26445	0.00000
O	-1.11357	-0.09153	0.00000
H	0.10347	1.49814	0.00000
H	-1.04998	-1.05849	0.00000

H_2O

O	0.00000	0.00000	0.11568
H	0.00000	0.76648	-0.46273
H	0.00000	-0.76648	-0.46273

CH_3OH

C	0.66286	-0.02061	0.00000
H	1.02454	-0.54695	-0.89318
H	1.08116	0.98744	-0.00137
H	1.02473	-0.54462	0.89448
O	-0.74484	0.12207	0.00000
H	-1.14887	-0.74879	0.00002

Reaction R7

RC-FFA

C	2.00453	0.51052	-0.00046
O	1.66464	-0.65530	0.00076
H	3.07461	0.77641	-0.00229
O	-1.06818	1.15990	0.00027
H	-0.07642	-0.98082	-0.00044
O	-1.05845	-1.09462	-0.00039
H	1.25443	1.31719	0.00057
C	-1.64150	0.09201	0.00003
H	-2.73483	-0.00785	-0.00036

TS-FFA

C	1.29462	0.41113	0.21512
O	1.27435	-0.76622	-0.26223
H	1.87827	1.17557	-0.30501
O	-0.37432	1.13329	-0.10832
H	0.10619	-1.13304	0.05296
O	-1.03758	-0.99731	0.15745
H	1.17595	0.56915	1.29513
C	-1.25512	0.23776	-0.06647
H	-2.29700	0.53690	-0.23013

HCO_2CH_2OH

C	-1.02132	-0.39258	0.39233
O	-1.47250	0.66835	-0.35961
H	-1.77162	-1.17919	0.35901
O	0.16446	-1.00827	-0.16750
H	-0.87920	1.41486	-0.20959
O	1.30004	0.89909	0.23267
H	-0.78352	-0.10956	1.42343
C	1.25297	-0.24229	-0.16537
H	2.10848	-0.79023	-0.57921

RC1(M)-FFA

Si	-1.81355	-0.12562	0.03398
O	-1.68310	0.36590	-1.53453
H	-2.17127	1.15403	-1.78161
O	-1.10106	-1.57876	0.19710
H	-0.17136	-1.65969	-0.07212
O	-1.12100	1.10145	0.90670
H	-1.24033	1.07561	1.85881
O	-3.36646	-0.26528	0.56125
H	-3.77507	-1.12780	0.46005
C	1.22418	1.90981	-0.36228
O	2.27173	1.85173	0.25433
H	0.85913	1.06085	-0.95821
H	0.61759	2.82665	-0.34617
C	2.73318	-1.44452	-0.03006
H	3.19229	-2.43788	0.04662
O	3.56670	-0.49430	0.31536
O	1.58627	-1.27042	-0.40048
H	3.10985	0.39260	0.27301

RC2(M)-FFA

Si	-2.31675	-0.12660	0.01112
O	-1.67770	1.39998	-0.00565

H	-2.11875	2.04184	0.55597
O	-1.19502	-1.12179	-0.63218
H	-0.26227	-0.94435	-0.43834
O	-2.74491	-0.39337	1.57802
H	-3.39750	-1.07872	1.73580
O	-3.68965	-0.31464	-0.87841
H	-3.56845	-0.54269	-1.80260
C	4.84939	-0.53824	0.12071
O	3.91707	-1.31608	0.08245
H	4.67888	0.54938	0.08629
H	5.88254	-0.91552	0.19048
C	1.58809	1.13400	-0.12810
H	0.61188	1.62862	-0.20468
O	1.44166	-0.19294	-0.09232
O	2.65557	1.70056	-0.07790
H	2.32709	-0.63438	-0.02637

RC3(M)-FFA

Si	-0.44723	-1.12651	-0.05584
O	-1.28365	-2.12482	-1.06126
H	-0.75750	-2.64582	-1.67198
O	-1.45639	-0.86082	1.22943
H	-1.88872	-1.64164	1.58345
O	0.98672	-1.81664	0.26541
H	1.72938	-1.23021	0.50794
O	-0.14939	0.38441	-0.66742
H	-0.90386	1.00856	-0.70447
C	-2.89330	1.95933	0.57713
O	-2.28446	2.10734	-0.46235
H	-3.73953	2.62146	0.82634
H	-2.61955	1.16280	1.28804
C	3.09699	1.10153	0.12999
H	4.01457	1.70061	0.18121
O	2.98146	0.03917	0.71266
O	2.18837	1.68077	-0.61956
H	1.34300	1.15494	-0.64677

TSM1-FFA

Si	-1.88633	-0.03130	0.02638
O	-1.54995	1.34840	-0.81729
H	-1.92317	2.16066	-0.46707
O	-1.19990	-1.28291	-0.75962
H	-0.23865	-1.23256	-0.89117
O	-1.29185	0.25219	1.54248
H	-1.60799	-0.31990	2.24528
O	-3.49172	-0.34772	0.18797
H	-3.90271	-0.86879	-0.50522
C	1.59744	1.22880	-0.09520
O	2.84115	1.46061	-0.11051
H	1.09024	0.93525	0.82899
H	0.96927	1.64841	-0.88259
C	2.48677	-1.27579	-0.08619
H	2.55843	-2.36250	-0.22687
O	3.39153	-0.72016	0.60368
O	1.51099	-0.67872	-0.62177
H	3.27584	0.50602	0.41809

TSM2-FFA

Si	-2.23295	-0.04342	0.01304
O	-1.42784	1.35026	-0.38254

H	-1.82228	2.16269	-0.05609
O	-1.21749	-1.28149	-0.29242
H	-0.27206	-1.15793	-0.11269
O	-2.70674	0.17211	1.57452
H	-3.43219	-0.37381	1.88480
O	-3.60599	-0.31747	-0.85214
H	-3.50162	-0.80363	-1.67294
C	4.14528	-0.01286	0.32916
O	3.74744	-1.14541	-0.07452
H	3.96851	0.30021	1.36538
H	5.00264	0.45008	-0.16609
C	1.70621	0.68970	-0.25263
H	0.82912	1.27520	-0.55175
O	1.47965	-0.52799	0.10159
O	2.83939	1.21883	-0.25769
H	2.51297	-1.05686	0.13318

TSM3-FFA

Si	-2.25540	-0.12780	0.03579
O	-3.22801	1.10046	-0.47079
H	-3.99645	0.85585	-0.99056
O	-1.39488	0.51966	1.29912
H	-1.90122	1.08045	1.89185
O	-3.25576	-1.36659	0.45636
H	-2.87918	-2.24787	0.40618
O	-1.17687	-0.71882	-1.02878
H	-0.34120	-0.23666	-1.17795
C	1.50681	1.05519	0.11591
O	1.23786	0.62247	-1.08377
H	2.13638	1.94625	0.22668
H	0.80898	0.83700	0.93005
C	4.03566	-0.16128	0.50451
H	4.24184	0.40342	1.42549
O	4.86939	-0.66375	-0.19243
O	2.70742	-0.24602	0.25597
H	2.17846	-0.19202	-0.82064

PC1(M)-FFA

Si	-1.78656	0.08525	0.06231
O	-0.73696	0.10108	1.33365
H	-0.74867	-0.66469	1.91297
O	-1.20612	1.13693	-1.05260
H	-0.27245	1.02183	-1.26996
O	-1.84235	-1.48829	-0.42645
H	-2.61113	-1.76014	-0.93253
O	-3.32453	0.54405	0.40696
H	-3.52377	1.48188	0.37113
C	2.19976	1.04923	0.16352
O	3.55807	0.85068	0.22915
H	1.68023	0.87215	1.10933
H	2.01769	2.05504	-0.20947
C	1.57034	-1.11792	-0.51882
H	0.99652	-1.69088	-1.25667
O	2.13325	-1.59565	0.43651
O	1.56081	0.18611	-0.82315
H	3.71545	0.02424	0.70224

PC2(M)-FFA

Si	-2.26314	-0.03481	0.00344
O	-1.40945	1.18344	-0.72909

H	-1.79973	2.05822	-0.66165
O	-1.27442	-1.32547	0.09162
H	-0.32556	-1.17420	0.24995
O	-2.78464	0.61417	1.42412
H	-3.53420	0.18621	1.84307
O	-3.61647	-0.50904	-0.80670
H	-3.49846	-1.20887	-1.45263
C	3.90465	0.30182	0.36688
O	4.18943	-0.91249	-0.21097
H	3.61559	0.21631	1.41961
H	4.76671	0.95258	0.24138
C	1.63917	0.44017	-0.24007
H	0.86261	1.02855	-0.74163
O	1.41914	-0.61720	0.32736
O	2.83139	1.00556	-0.31401
H	3.49415	-1.53523	0.03425

PC3(M)-FFA

Si	2.23363	0.14267	-0.00086
O	3.22976	-1.15862	0.16017
H	4.04842	-1.13561	-0.33970
O	1.28418	0.12715	1.35597
H	1.73160	-0.11257	2.17089
O	3.21797	1.45478	-0.14175
H	2.84180	2.22247	-0.57794
O	1.23069	0.15551	-1.28641
H	0.40067	-0.34317	-1.22787
C	-1.74273	-0.68612	0.45909
O	-1.15076	-1.20568	-0.69409
H	-2.27277	-1.46863	1.01859
H	-0.93410	-0.25972	1.05048
C	-3.95726	0.09921	0.14405
H	-4.19445	-0.93737	0.45182
O	-4.78512	0.90887	-0.15467
O	-2.63886	0.37022	0.14749
H	-1.79490	-1.65913	-1.24672

RC1(T)-FFA

Si	0.98135	0.58049	1.69647
O	1.71931	1.74417	2.57690
H	1.49272	1.76659	3.50870
O	-0.18487	1.22788	0.72839
O	2.10999	-0.06932	0.70222
O	0.31860	-0.49770	2.71891
H	-0.39668	-1.05066	2.35436
Si	2.36851	-0.77624	-0.73704
Si	-0.69432	1.54156	-0.77781
O	3.72874	-1.68154	-0.77651
O	2.58218	0.49529	-1.78833
H	2.98259	0.28245	-2.63512
O	1.10194	-1.72444	-1.17321
H	0.26283	-1.25426	-1.32075
O	-1.08456	0.04446	-1.39847
H	-1.58332	0.03842	-2.22007
O	-2.08741	2.41370	-0.77046
H	-2.00640	3.36693	-0.84795
O	0.40545	2.32827	-1.68803
H	1.27227	1.89538	-1.77766
H	3.66796	-2.59562	-0.49270
C	-3.87105	0.37983	0.32201

O	-4.18382	-0.50186	-0.45520
H	-2.98658	0.27695	0.96943
H	-4.47355	1.29668	0.39797
C	-1.65487	-2.55709	0.41507
H	-0.88718	-3.33627	0.35088
O	-2.50589	-2.62173	-0.57975
O	-1.69661	-1.73198	1.31189
H	-3.15109	-1.86612	-0.51912

RC2(T)-FFA

Si	-0.45122	0.46707	1.60223
O	0.61731	1.25407	2.52658
H	1.50916	1.36479	2.14814
O	-1.01335	1.34668	0.32938
O	0.20362	-0.90718	0.98227
O	-1.78330	0.10206	2.51107
H	-1.66985	0.06531	3.46288
Si	0.01782	-2.08419	-0.12675
Si	-2.22364	0.99362	-0.72343
O	1.08118	-3.31176	0.06274
O	0.38487	-1.35916	-1.58861
H	0.74926	-1.94765	-2.25616
O	-1.49739	-2.69230	-0.12574
H	-2.21775	-2.03912	-0.14184
O	-3.05901	-0.29704	-0.07447
H	-3.25590	-0.21198	0.86877
O	-3.13212	2.33677	-0.90714
H	-3.69049	2.39355	-1.68496
O	-1.66261	0.51496	-2.18143
H	-1.02631	-0.21900	-2.17127
H	0.78127	-4.08131	0.55098
C	1.61724	1.16076	-2.00382
O	2.76855	0.90361	-2.30414
H	1.31332	1.29713	-0.95621
H	0.84868	1.28101	-2.78179
C	3.94916	0.82995	0.82435
H	4.60816	0.63119	1.67797
O	4.50531	0.49819	-0.31189
O	2.83398	1.30850	0.94376
H	3.87422	0.67148	-1.06741

RC3(T)-FFA

Si	-0.70927	1.11705	-0.46984
O	-0.38142	1.18174	1.17141
H	-1.17680	1.19863	1.72532
O	0.24780	-0.10369	-1.01310
O	-2.28968	0.76545	-0.66405
O	-0.37649	2.49625	-1.24952
H	0.56174	2.74165	-1.26109
Si	-3.38778	-0.09517	0.19670
Si	0.77910	-1.49499	-0.33158
O	-4.93516	0.31838	-0.13226
O	-3.06165	0.37360	1.75815
H	-3.67427	0.09828	2.44316
O	-3.22077	-1.69622	-0.06392
H	-2.32017	-2.04175	-0.19954
O	-0.53917	-2.50977	-0.34191
H	-0.34838	-3.45030	-0.30226
O	1.97407	-2.24526	-1.12728
H	2.89127	-1.97321	-0.93848

O	1.28554	-1.14220	1.20380
H	0.77039	-0.41809	1.59333
H	-5.37766	-0.18418	-0.81966
C	4.48977	-1.14731	0.94912
O	4.49256	-1.40882	-0.23656
H	5.41947	-0.83948	1.45715
H	3.56496	-1.20727	1.54503
C	2.70093	2.09841	0.34698
O	2.42846	2.63301	-0.70244
O	3.93746	1.73547	0.69265
H	1.97391	1.84931	1.12889
H	4.53021	1.95970	-0.04206

TST1-FFA

Si	-0.74365	-0.34779	1.77332
O	-1.72734	-1.19697	2.76296
H	-1.87872	-0.83634	3.63871
O	-0.08404	-1.40508	0.70859
O	-1.58402	0.76231	0.90239
O	0.39141	0.39207	2.68010
H	0.99581	0.97513	2.19431
Si	-1.96914	1.34163	-0.56486
Si	-0.02329	-1.99081	-0.80703
O	-2.86792	2.70584	-0.49756
O	-2.90101	0.15237	-1.25960
H	-3.43311	0.41825	-2.01404
O	-0.62316	1.66728	-1.44383
H	-0.03381	0.91372	-1.62299
O	0.78859	-0.79083	-1.63853
H	1.13332	-1.02776	-2.50402
O	0.89977	-3.33499	-0.92191
H	0.46929	-4.18284	-0.79307
O	-1.49839	-2.30050	-1.42524
H	-2.15332	-1.58299	-1.37442
H	-2.40904	3.54524	-0.56553
C	3.30760	-0.14666	0.60780
O	4.27597	0.27656	-0.09153
H	2.45547	-0.63872	0.13417
H	3.48427	-0.36901	1.66211
C	2.20358	2.08452	-0.25099
H	1.55723	2.96651	-0.31712
O	2.90980	1.80108	-1.26381
O	2.18822	1.42079	0.82538
H	3.70756	0.94978	-0.89821

TST2-FFA

Si	-0.30448	0.21799	1.62883
O	0.96823	-0.10067	2.57789
H	1.79387	-0.31251	2.10365
O	0.07977	1.33157	0.47159
O	-0.85092	-1.10863	0.84132
O	-1.54019	0.81268	2.54528
H	-1.32389	1.06151	3.44658
Si	-1.76739	-1.77758	-0.32504
Si	-0.87530	1.96092	-0.70664
O	-1.97930	-3.38715	-0.14555
O	-0.85197	-1.56545	-1.70645
H	-1.04121	-2.16690	-2.43196
O	-3.22745	-1.05846	-0.44325
H	-3.21315	-0.08658	-0.43914

O	-2.45484	1.68373	-0.24196
H	-2.65268	1.90030	0.67815
O	-0.50558	3.54566	-0.83849
H	-0.72094	3.98515	-1.66354
O	-0.65180	1.23348	-2.14915
H	-0.75212	0.26736	-2.18421
H	-2.75559	-3.68078	0.33582
C	2.27506	-0.38134	-1.14083
O	3.20803	-0.92806	-1.79569
H	2.26301	0.69654	-0.96898
H	1.32855	-0.91612	-1.04476
C	4.21765	-0.31088	0.70486
H	4.75692	-0.28978	1.66177
O	4.89458	-0.12633	-0.34676
O	2.97015	-0.51467	0.74197
H	4.15176	-0.46523	-1.32369

TST3-FFA

Si	-0.72389	1.14762	-0.42501
O	-0.43669	1.16666	1.22377
H	-1.24682	1.15403	1.75607
O	0.21263	-0.08568	-0.98351
O	-2.30510	0.82268	-0.66360
O	-0.35559	2.53843	-1.16761
H	0.58521	2.76394	-1.13703
Si	-3.40760	-0.08850	0.13713
Si	0.79069	-1.44134	-0.27654
O	-4.95280	0.30497	-0.22348
O	-3.13094	0.33186	1.72175
H	-3.75343	0.01920	2.38136
O	-3.20574	-1.67872	-0.16715
H	-2.29769	-2.02039	-0.24339
O	-0.49441	-2.49272	-0.24016
H	-0.28760	-3.42542	-0.14241
O	2.00466	-2.17849	-1.06014
H	2.90604	-1.83088	-0.94076
O	1.31008	-1.02579	1.24237
H	0.76040	-0.31310	1.61271
H	-5.36582	-0.18169	-0.94000
C	4.35294	-0.63525	0.94159
O	4.43952	-0.95021	-0.31596
H	5.26869	-0.42531	1.50091
H	3.45047	-0.90635	1.50014
C	2.90718	1.80585	0.42032
O	2.43583	2.33165	-0.55751
O	4.03384	1.08570	0.37409
H	2.47389	1.87396	1.42687
H	4.27482	0.25687	-0.50700

PC1(T)-FFA

Si	0.62585	0.28710	1.78230
O	1.48695	1.21457	2.81416
H	1.68125	0.84629	3.67816
O	-0.10685	1.28832	0.71508
O	1.58569	-0.73497	0.93102
O	-0.45535	-0.57680	2.65249
H	-1.01400	-1.16853	2.13317
Si	2.27268	-1.11237	-0.49312
Si	-0.19240	1.85759	-0.80643
O	3.39627	-2.29346	-0.36717

O	3.04263	0.27957	-0.97846
H	3.72183	0.17331	-1.64971
O	1.13759	-1.60272	-1.56952
H	0.44287	-0.94767	-1.75882
O	-0.68474	0.54254	-1.70757
H	-1.10352	0.72859	-2.55260
O	-1.36006	2.98833	-0.98606
H	-1.12875	3.90238	-0.80803
O	1.23396	2.46352	-1.31179
H	2.00717	1.88752	-1.18794
H	3.11586	-3.19202	-0.55185
C	-3.16561	-0.20409	0.54361
O	-4.44516	-0.70573	0.57254
H	-2.98499	0.47259	-0.29587
H	-2.95543	0.27939	1.49503
C	-2.12805	-1.91305	-0.71155
H	-1.29259	-2.62317	-0.72953
O	-2.90794	-1.74395	-1.61833
O	-2.16515	-1.25947	0.45344
H	-4.67635	-0.98613	-0.32142

PC2(T)-FFA

Si	-0.57135	0.24936	1.65691
O	0.44755	1.06963	2.63080
H	1.13777	1.55179	2.16087
O	-1.13090	1.23651	0.46241
O	0.11560	-1.06390	0.96951
O	-1.83451	-0.29406	2.56395
H	-2.01876	0.18562	3.37468
Si	0.23914	-2.01318	-0.34962
Si	-2.20591	0.92204	-0.73947
O	1.44965	-3.10485	-0.21147
O	0.68485	-0.97566	-1.57516
H	1.16547	-1.36074	-2.31313
O	-1.15990	-2.78767	-0.66907
H	-1.94773	-2.21872	-0.66285
O	-2.91817	-0.54441	-0.37387
H	-3.29335	-0.61139	0.51250
O	-3.27919	2.15212	-0.78304
H	-3.72997	2.32100	-1.61278
O	-1.47682	0.76584	-2.18709
H	-0.69657	0.18695	-2.20027
H	1.23749	-3.96267	0.16239
C	3.21419	0.30132	0.43273
O	4.43394	0.92934	0.33102
H	3.07567	-0.49378	-0.30531
H	3.10120	-0.07945	1.44569
C	1.93236	1.69866	-0.96889
H	1.01329	2.29296	-1.02627
O	2.69007	1.49854	-1.88751
O	2.10516	1.22454	0.27111
H	4.59128	1.12541	-0.60075

PC3(T)-FFA

Si	0.68239	-1.11453	-0.25675
O	0.54755	-0.99511	1.40199
H	1.39343	-1.02981	1.87265
O	-0.26544	0.11883	-0.80934
O	2.24241	-0.88198	-0.67204
O	0.17916	-2.52675	-0.86309

H	-0.76768	-2.72961	-0.79008
Si	3.47255	-0.02173	-0.01259
Si	-0.71656	1.53493	-0.12052
O	4.94685	-0.50740	-0.52611
O	3.34792	-0.39170	1.60207
H	4.06081	-0.11307	2.18034
O	3.32124	1.57072	-0.33914
H	2.42452	1.94748	-0.32769
O	0.64450	2.48532	-0.12737
H	0.51771	3.42050	0.05168
O	-1.88707	2.32230	-0.92496
H	-2.79296	1.99782	-0.80085
O	-1.26460	1.20596	1.40530
H	-0.70298	0.54904	1.84797
H	5.30218	-0.06378	-1.29923
C	-4.49871	0.16744	0.65047
O	-4.38708	1.09608	-0.38509
H	-5.50450	0.14481	1.07295
H	-3.75477	0.45435	1.39809
C	-2.98777	-1.55380	0.11579
O	-2.66413	-2.57919	-0.42342
O	-4.26767	-1.15467	0.17349
H	-2.28664	-0.86758	0.61327
H	-5.05656	0.92753	-1.05706

Reaction R8

RC-FW

C	0.96176	0.56175	0.00195
O	1.32507	-0.59059	0.00478
H	0.80144	1.12352	0.93964
H	0.77374	1.11101	-0.93767
O	-1.73076	0.00443	-0.02972
H	-1.43489	-0.91062	-0.00450
H	-2.66537	-0.00512	0.19037

TS-FW

C	0.34550	0.62851	0.00071
O	1.02804	-0.48236	0.02692
H	0.25841	1.23096	0.92005
H	0.33031	1.23236	-0.91661
O	-1.12694	-0.16706	-0.11034
H	-0.23404	-0.90374	-0.05211
H	-1.63650	-0.13529	0.71181

$CH_2(OH)_2$

C	0.00003	0.52966	0.00001
O	1.16298	-0.24672	0.09447
H	0.00066	1.15834	0.89652
H	-0.00077	1.15815	-0.89666
O	-1.16299	-0.24673	-0.09447
H	1.24308	-0.77348	-0.70751
H	-1.24309	-0.77342	0.70765

RC1(M)-FW

Si	1.20726	-0.00706	-0.01195
O	1.12732	-0.45486	1.57260
H	1.73054	-1.14369	1.86006
O	0.43793	1.46988	-0.04513
H	0.74632	2.10556	0.60694
O	2.79503	0.09348	-0.42403
H	3.01107	-0.06730	-1.34517
O	0.46878	-0.98857	-1.07030
H	-0.46252	-1.25042	-0.91873
C	-2.48092	-0.81776	0.54580
O	-2.16008	-1.44798	-0.44276
H	-3.53884	-0.65080	0.79710
H	-1.73313	-0.42497	1.25304
O	-2.37202	1.68860	-0.11042
H	-2.73969	1.85628	-0.98158
H	-1.40559	1.69642	-0.21890

RC2(M)-FW

Si	-0.64465	-0.66587	-0.00996
O	0.41123	-1.09170	1.19361
H	0.27911	-1.96677	1.56578
O	0.03884	0.63355	-0.75893
H	1.01109	0.65746	-0.84327
O	-0.80390	-2.02397	-0.92928
H	-1.61294	-2.09251	-1.44068
O	-2.13797	-0.20919	0.46788
H	-2.26294	0.75147	0.57076
O	-1.72985	2.54353	0.22872
H	-0.97516	2.20529	-0.28315
H	-2.22695	3.12214	-0.35376
C	3.21212	0.30501	0.42883
H	2.51663	-0.12848	1.16605
H	4.28611	0.34744	0.67890
O	2.81382	0.72229	-0.63877

TSM1-FW

Si	1.19434	-0.04536	-0.00063
O	1.45429	0.25491	1.59732
H	2.12872	-0.26571	2.03866
O	0.31709	1.31312	-0.47769
H	0.70500	2.15333	-0.21567
O	2.66552	-0.11942	-0.72829
H	2.71431	-0.64846	-1.52789
O	0.33267	-1.34619	-0.39362
H	-0.65983	-1.40151	-0.25027
C	-2.40230	-0.02696	0.65710
O	-2.24451	-1.13878	-0.08772
H	-3.39232	0.12809	1.09782
H	-1.59387	0.23265	1.35620
O	-2.33511	0.96275	-0.51982
H	-2.33528	-0.08654	-0.97340
H	-1.39330	1.27371	-0.58069

TSM2-FW

Si	1.42614	-0.03346	-0.03330
O	2.17542	1.04407	0.96687

H	2.92094	0.70927	1.46924
O	0.59042	0.91743	-1.10599
H	1.04924	1.71277	-1.38617
O	2.63331	-0.92639	-0.72050
H	2.38277	-1.81088	-0.99579
O	0.37540	-1.07608	0.62960
H	-0.53480	-0.76472	0.85243
C	-2.45403	0.65743	0.01453
O	-2.10876	-0.16073	1.00052
H	-3.04958	1.54446	0.27392
H	-1.73075	0.82610	-0.79004
O	-3.51390	-0.38817	-0.62676
H	-4.43563	-0.12006	-0.49965
H	-3.05911	-0.85414	0.30512

TSM3-FW

Si	1.50961	-0.00865	-0.01416
O	1.79143	-1.54381	-0.51824
H	2.60108	-1.71048	-1.00548
O	0.42251	-0.17470	1.24161
H	0.59667	-0.88281	1.86729
O	2.96019	0.62393	0.41559
H	3.03687	1.58066	0.41851
O	0.80163	1.00959	-1.07454
H	-0.16481	1.03076	-1.10642
O	-1.87136	0.55422	-0.04021
H	-1.24996	0.28478	0.67250
H	-2.90098	0.88974	0.35687
C	-3.04686	-0.59670	-0.31443
H	-2.66838	-1.49038	0.20849
H	-3.01276	-0.69389	-1.40882
O	-3.99081	0.11739	0.23603

PC1(M)-FW

Si	-1.26881	0.01844	-0.00312
O	-1.59537	-0.21305	1.59292
H	-2.33802	0.26962	1.96174
O	-0.33324	-1.29840	-0.41189
H	-0.62197	-2.14030	-0.04927
O	-2.71626	0.07770	-0.77987
H	-2.73206	0.54249	-1.61934
O	-0.42871	1.34624	-0.41029
H	0.53257	1.38501	-0.23090
C	2.61048	-0.11091	0.48897
O	2.26665	1.20572	0.06230
H	3.65555	-0.13256	0.81011
H	1.94839	-0.30427	1.34022
O	2.47283	-1.04577	-0.52058
H	2.80556	1.41837	-0.70798
H	1.52336	-1.21052	-0.65551

PC2(M)-FW

Si	1.39416	0.03124	-0.00930
O	1.12739	1.30404	1.00847
H	1.68074	1.34860	1.79120
O	0.72737	0.49148	-1.44776

H	0.92453	1.38515	-1.73725
O	3.02308	-0.20568	-0.04244
H	3.32184	-1.08595	-0.28028
O	0.70150	-1.37944	0.42335
H	-0.26870	-1.42756	0.35092
C	-2.31042	0.27884	-0.08332
O	-2.05523	-1.10074	0.12715
H	-1.71592	0.79511	0.67716
H	-1.98802	0.58598	-1.08048
O	-3.66950	0.57430	0.00358
H	-3.96503	0.41835	0.90646
H	-2.48210	-1.60170	-0.57642

PC3(M)-FW

Si	-1.38367	0.03757	0.00248
O	-1.31870	1.46641	-0.80980
H	-2.03633	1.65953	-1.41660
O	-0.39561	0.25803	1.32108
H	-0.45732	1.10712	1.76562
O	-2.96639	-0.22821	0.35448
H	-3.22290	-1.13771	0.52202
O	-0.80532	-1.27652	-0.77326
H	0.15418	-1.41540	-0.69542
O	1.85112	-0.97022	0.11595
H	1.37533	-0.58533	0.87096
H	4.18931	-0.06756	0.47227
C	2.54381	0.07103	-0.53112
H	1.87433	0.90188	-0.77752
H	2.94807	-0.37217	-1.44742
O	3.54540	0.62020	0.27382

RC1(T)-FW

Si	0.11264	1.27396	0.21243
O	0.58554	1.38326	1.77940
H	0.35612	0.61759	2.31889
O	0.76931	-0.02677	-0.53393
O	-1.51666	1.22474	0.09480
O	0.71611	2.58283	-0.58323
H	0.43628	3.45284	-0.28975
Si	-2.81570	0.25017	-0.08712
Si	0.58953	-1.61515	-0.10182
O	-4.21346	1.09632	-0.06195
O	-2.75152	-0.73520	1.25361
H	-3.53584	-1.25979	1.43396
O	-2.76232	-0.60593	-1.47578
H	-2.03432	-1.24422	-1.56854
O	-0.50635	-2.30455	-1.14637
H	-0.15093	-2.94694	-1.76561
O	1.99044	-2.40702	-0.19779
H	2.82239	-1.90390	-0.05570
O	-0.07388	-1.61194	1.40405
H	-1.04112	-1.54269	1.47321
H	-4.63759	1.25829	-0.90732
C	4.05997	0.26966	0.67047
O	4.17869	-0.84093	0.18826
H	4.92093	0.94800	0.74722
H	3.10282	0.62637	1.08187
O	3.46123	1.98921	-1.19566

H	3.42194	1.39612	-1.95093
H	2.55181	2.30241	-1.07228

RC2(T)-FW

Si	-0.37160	-1.45202	-0.79213
O	0.19175	-2.47222	0.37301
H	-0.21447	-3.33925	0.44098
O	-1.89163	-0.92782	-0.47348
O	0.65854	-0.19836	-0.78190
O	-0.37916	-2.28142	-2.20060
H	-0.90825	-1.94169	-2.92491
Si	1.03263	1.37712	-0.51270
Si	-2.57626	0.22825	0.47001
O	2.52307	1.76094	-0.99041
O	0.85984	1.46511	1.16805
H	1.15895	2.29224	1.55873
O	-0.01272	2.39092	-1.23739
H	-0.94993	2.29032	-1.00303
O	-2.63780	1.63096	-0.43138
H	-3.27551	1.65163	-1.14989
O	-4.07089	-0.31161	0.84847
H	-4.48684	0.05114	1.63323
O	-1.72180	0.55536	1.81220
H	-0.82678	0.92986	1.73442
H	3.26247	1.24123	-0.60801
C	3.95243	-0.98294	0.45154
O	4.30330	0.17420	0.31792
H	3.15656	-1.41916	-0.17173
H	4.44800	-1.64720	1.17298
O	2.01610	-1.09773	2.15877
H	1.66984	-0.20112	2.05555
H	1.35574	-1.66389	1.73374

RC3(T)-FW

Si	-0.26523	-0.29208	1.73820
O	0.51184	-1.58207	2.32607
H	0.92548	-2.21430	1.69992
O	0.74982	0.88726	1.19859
O	-1.18957	-0.71697	0.44298
O	-1.17115	0.36904	2.93093
H	-1.33820	-0.19532	3.68870
Si	-2.05914	-0.24631	-0.84571
Si	1.13294	1.77881	-0.10024
O	-3.33192	-1.21664	-1.17706
O	-0.97569	-0.42756	-2.10515
H	-1.34982	-0.43170	-2.99015
O	-2.59899	1.28893	-0.70717
H	-1.93443	1.95613	-0.46926
O	-0.18127	2.77670	-0.33864
H	-0.07180	3.46814	-0.99717
O	2.52233	2.60587	0.13737
H	2.72290	2.87390	1.03659
O	1.39324	0.89372	-1.45992
H	0.60827	0.44395	-1.82833
H	-4.17982	-0.97594	-0.79777
O	3.12376	-1.30421	-1.76279
H	2.71011	-0.43108	-1.66117
H	3.96611	-1.25954	-1.30429

C	1.39113	-2.96089	-0.72437
H	1.82863	-3.56657	-1.53025
H	0.71365	-2.14524	-1.02284
O	1.61412	-3.21444	0.44363

TST1-FW

Si	-0.02260	-0.67135	1.61851
O	0.99580	-1.89840	1.80878
H	1.66290	-2.08676	1.08028
O	0.76575	0.74587	1.25849
O	-1.05287	-0.89599	0.35221
O	-0.89527	-0.44991	2.98693
H	-0.64847	-1.01181	3.72468
Si	-2.18417	-0.37375	-0.68188
Si	0.87051	1.82276	0.05723
O	-3.34762	-1.46623	-1.02843
O	-1.30841	-0.14931	-2.09126
H	-1.82058	-0.03221	-2.89558
O	-2.89802	1.00954	-0.18171
H	-2.29131	1.71422	0.09252
O	-0.54952	2.68486	0.07349
H	-0.57597	3.48568	-0.45681
O	2.19542	2.76469	0.21163
H	2.54678	2.89087	1.09566
O	1.03357	1.11261	-1.43236
H	0.20899	0.73169	-1.80410
H	-4.12669	-1.47836	-0.46837
O	2.82266	-0.82910	-1.77620
H	2.24845	-0.01905	-1.70578
H	3.20932	-1.13560	-0.75461
C	2.01756	-2.07153	-1.38136
H	2.24509	-2.81888	-2.14883
H	0.95329	-1.79261	-1.37660
O	2.61233	-2.24179	-0.18262

TST2-FW

Si	0.18443	1.28462	-0.74270
O	-0.31323	1.97535	0.68980
H	0.25738	1.75870	1.43890
O	1.80822	1.06798	-0.68836
O	-0.56098	-0.14600	-0.94027
O	-0.28297	2.32503	-1.90369
H	-0.41164	1.97984	-2.78944
Si	-0.84316	-1.64781	-0.31051
Si	2.65777	0.09289	0.32746
O	-2.35511	-2.14000	-0.54230
O	-0.49982	-1.39873	1.32565
H	-0.83752	-2.08356	1.90999
O	0.20544	-2.73029	-0.93493
H	1.13545	-2.51218	-0.77614
O	2.77881	-1.42336	-0.34324
H	3.35478	-1.50452	-1.10864
O	4.11226	0.80167	0.53361
H	4.67254	0.48841	1.24640
O	1.85211	-0.05891	1.74257
H	1.07620	-0.65575	1.75601
H	-3.02258	-1.49490	-0.17201
C	-3.65839	1.00061	0.07478

O	-3.77975	-0.24477	0.57373
H	-3.00795	1.12609	-0.80320
H	-4.57994	1.58674	-0.00622
O	-2.91658	1.57663	1.28753
H	-3.09688	0.48133	1.52564
H	-1.96326	1.77359	1.08984

TST3-FW

Si	0.07996	1.34689	-0.07663
O	0.61535	1.56147	1.45945
H	0.52421	0.76755	2.00187
O	0.68765	-0.04975	-0.69551
O	-1.56398	1.25128	-0.13494
O	0.53275	2.64003	-0.97417
H	-0.18876	3.11872	-1.38720
Si	-2.78410	0.17490	-0.01619
Si	0.68592	-1.57169	-0.05257
O	-4.24074	0.92049	0.01675
O	-2.51920	-0.57796	1.44809
H	-3.25168	-1.09664	1.79068
O	-2.80644	-0.89925	-1.24733
H	-2.05477	-1.51439	-1.30555
O	-0.46050	-2.45775	-0.87501
H	-0.12258	-3.17428	-1.41766
O	2.12922	-2.27336	-0.18590
H	2.92063	-1.67477	-0.27495
O	0.18116	-1.42154	1.51212
H	-0.77772	-1.33680	1.64960
H	-4.78317	0.82985	-0.76952
C	3.86895	0.46110	0.60785
O	4.02977	-0.45598	-0.34770
H	4.77218	0.96005	0.98516
H	3.13646	0.25875	1.39838
O	3.14410	1.49179	-0.32808
H	3.44004	0.62157	-0.98838
H	3.59349	2.33662	-0.47639

PC1(T)-FW

Si	-0.02104	-1.27455	-0.55157
O	-0.88672	-1.70621	0.79707
H	-0.73748	-1.10576	1.53956
O	-0.48416	0.20462	-1.06913
O	1.57248	-1.24544	-0.16947
O	-0.34084	-2.34462	-1.73558
H	-0.03018	-3.24541	-1.62822
Si	2.79647	-0.24559	0.24245
Si	-0.58004	1.59823	-0.19059
O	4.20699	-1.05294	0.41377
O	2.33109	0.34721	1.72915
H	3.01057	0.80016	2.23530
O	3.02549	0.95418	-0.84087
H	2.31189	1.60492	-0.94999
O	0.67045	2.58110	-0.66902
H	0.43806	3.34436	-1.20335
O	-1.98686	2.35797	-0.43304
H	-2.77024	1.77281	-0.46547
O	-0.33193	1.18514	1.38662
H	0.58844	1.09215	1.68751

H	4.83642	-0.98570	-0.30736
C	-4.03954	-0.36708	0.88302
O	-3.88470	0.40604	-0.30460
H	-5.08312	-0.33319	1.20943
H	-3.39663	0.12833	1.62006
O	-3.72121	-1.69691	0.68809
H	-4.27241	-0.08374	-1.03793
H	-2.75401	-1.80077	0.65429

PC2(T)-FW

Si	0.03058	-1.27705	0.62368
O	-0.55182	-1.92834	-0.77673
H	-0.05661	-1.71043	-1.57317
O	1.67076	-1.24104	0.60043
O	-0.52222	0.24652	0.81821
O	-0.55825	-2.23025	1.80601
H	-0.56493	-1.88140	2.69924
Si	-0.61129	1.77658	0.23394
Si	2.68658	-0.29695	-0.27857
O	-2.08330	2.42285	0.42653
O	-0.21231	1.58292	-1.39025
H	-0.38261	2.35006	-1.94360
O	0.48011	2.75125	0.95476
H	1.39332	2.44246	0.85432
O	2.90161	1.14970	0.52067
H	3.38814	1.10061	1.34838
O	4.08184	-1.13207	-0.42214
H	4.70949	-0.84565	-1.08850
O	2.04425	0.04812	-1.73895
H	1.30730	0.68900	-1.76546
H	-2.80615	1.82919	0.14782
C	-3.79570	-0.90291	-0.01857
O	-3.72933	0.42895	-0.52360
H	-3.15793	-0.89503	0.87118
H	-4.82818	-1.13667	0.25810
O	-3.40558	-1.83885	-0.95707
H	-4.20033	0.45522	-1.36300
H	-2.43556	-1.89427	-0.98363

PC3(T)-FW

Si	-0.21051	-0.22123	1.77315
O	0.82939	-1.32589	2.34406
H	1.53517	-1.63400	1.74193
O	0.57087	1.09080	1.14779
O	-1.12875	-0.81893	0.55203
O	-1.17643	0.26083	3.00316
H	-0.96569	-0.10233	3.86575
Si	-2.10561	-0.61938	-0.72832
Si	0.82397	1.83008	-0.27607
O	-3.24074	-1.78352	-0.89064
O	-1.05856	-0.77957	-2.01903
H	-1.45807	-0.92001	-2.88119
O	-2.84951	0.83568	-0.71235
H	-2.26804	1.60188	-0.57901
O	-0.60574	2.62060	-0.61000
H	-0.58393	3.23830	-1.34591
O	2.09858	2.84857	-0.19375
H	2.30613	3.22342	0.66452

O	1.16338	0.79749	-1.50882
H	0.41235	0.26576	-1.83892
H	-4.08854	-1.63406	-0.46682
O	2.98902	-1.31846	-1.72639
H	2.55922	-0.44857	-1.65832
H	3.62866	-2.02177	0.53480
C	2.31860	-2.20668	-0.90656
H	2.59057	-3.21456	-1.23392
H	1.23064	-2.07855	-0.93437
O	2.66849	-2.03859	0.46496

Reaction R9

RC-FAM

C	-1.35252	-0.26112	-0.14093
O	-0.89291	0.96936	0.16511
O	1.76420	0.07524	-0.71845
H	1.23407	0.86056	-0.54869
O	-2.48056	-0.62420	0.06008
C	2.37853	-0.32264	0.49241
H	3.07905	0.43478	0.86632
H	1.63992	-0.53788	1.27698
H	2.93746	-1.23612	0.28181
H	-1.62504	1.47378	0.55017
H	-0.54743	-0.85579	-0.58940

TS1-FAM

C	-1.99996	-0.21223	0.15957
H	-2.81838	0.08222	-0.50093
H	-2.11627	-1.26646	0.42447
H	-2.03510	0.40150	1.06983
O	-0.77596	-0.03913	-0.53538
C	0.67234	-0.00518	0.38923
H	0.29796	-0.25968	1.38753
O	1.51154	-0.95584	-0.03916
O	0.87662	1.23454	0.03128
H	-0.23625	1.02709	-0.51941
H	1.97622	-0.59686	-0.80819

INT

C	-1.89557	-0.03295	0.08810
H	-1.95644	1.04667	-0.08802
H	-2.66613	-0.54252	-0.49017
H	-2.05549	-0.23350	1.15621
O	-0.65600	-0.56103	-0.34746
C	0.43740	-0.02725	0.30571
H	0.28662	-0.01467	1.39650
O	1.49504	-0.84416	-0.07110
O	0.66975	1.30924	-0.03637
H	0.77104	1.33953	-0.99674
H	2.29912	-0.46677	0.29891

TS2-FAM

C	-1.94386	0.18659	0.09312
H	-1.81097	1.27359	0.10823
H	-2.75877	-0.07809	-0.57840
H	-2.16947	-0.17101	1.10309

O	-0.77711	-0.44843	-0.42430
C	0.31731	-0.34782	0.33679
H	0.11273	-0.18918	1.40386
O	1.37939	-0.97141	-0.05314
O	1.12726	1.21062	0.02474
H	0.78679	1.62820	-0.77772
H	1.76277	0.17760	-0.21699

TS3-FAM

C	-0.64674	-0.36620	0.36040
O	-0.88504	1.30887	0.11746
O	0.72345	-0.03278	-0.54390
H	0.12502	1.00198	-0.47064
O	-1.44872	-1.09361	-0.14159
C	1.95502	-0.13363	0.15632
H	2.74613	0.24729	-0.49228
H	1.94242	0.44984	1.08608
H	2.15244	-1.18437	0.38522
H	-1.65952	1.38524	-0.45555
H	-0.27372	-0.36087	1.39110

CH_3OCHO

C	-0.44315	0.84232	0.33203
O	2.01738	-0.71460	0.00288
O	-0.86274	-0.12918	-0.48395
H	1.82855	-0.12177	-0.73185
O	-0.05188	1.90217	-0.07850
C	-1.12493	-1.40135	0.11592
H	-1.67915	-1.97493	-0.62516
H	-0.17939	-1.89604	0.35085
H	-1.73524	-1.29149	1.01835
H	2.84991	-0.41135	0.37330
H	-0.49829	0.58265	1.40341

RC1(M)-FAM

C	-2.33530	-1.70701	0.04426
O	-1.16627	-1.71856	0.40671
O	-3.00311	-0.66645	-0.36207
H	-2.94618	-2.61892	0.03331
H	-2.43124	0.17451	-0.39933
C	-1.63245	2.41173	0.55823
H	-1.38483	3.42186	0.21790
H	-2.63845	2.41864	0.98162
H	-0.91283	2.09298	1.31868
O	-1.64250	1.50751	-0.54373
H	-0.72633	1.37733	-0.85690
Si	1.63899	-0.08070	0.00639
O	3.19881	0.38663	0.17592
H	3.79996	-0.23988	0.58386
O	1.61556	-1.64331	-0.50008
H	0.77466	-2.09720	-0.36196
O	0.75452	0.14205	1.36625
H	-0.04377	-0.40688	1.37500
O	0.98220	0.95696	-1.12357
H	1.45601	1.06041	-1.95210

INTM

C	-2.12729	-0.57516	-0.45285
O	-1.13784	-1.32190	0.19205
O	-3.30551	-0.55978	0.29005

H	-2.26168	-1.04571	-1.43089
H	-3.45708	-1.45161	0.61798
C	-1.94245	1.68689	0.35214
H	-1.47467	2.60677	0.00159
H	-3.00499	1.84902	0.53734
H	-1.44898	1.36364	1.27450
O	-1.75169	0.74074	-0.70407
H	-0.77750	-0.83394	0.95448
Si	1.74621	0.00628	-0.02917
O	3.30676	0.46529	0.15921
H	3.94574	-0.23731	0.29311
O	1.70299	-1.56388	-0.49973
H	0.82074	-1.95423	-0.50730
O	0.91946	0.06303	1.43350
H	1.11967	0.81306	1.99819
O	1.06678	1.06817	-1.06771
H	0.10271	0.99867	-1.15280

RC2(M)-FAM

C	-2.82273	2.21194	-0.04273
H	-2.23315	3.13234	-0.10716
H	-3.49092	2.15906	-0.90305
H	-3.42176	2.22652	0.87385
O	-1.98313	1.06358	-0.09067
H	-1.32468	1.09137	0.62868
Si	1.49235	0.37813	-0.02509
O	0.40071	0.70919	1.20021
H	0.71612	0.61453	2.10220
O	2.78123	1.37297	0.15937
H	3.64162	0.99843	-0.04178
O	2.07961	-1.14394	0.02010
H	1.46443	-1.88754	-0.07634
O	0.61279	0.66380	-1.37910
H	-0.27466	1.02818	-1.25866
C	-1.09111	-1.92690	-0.30623
H	-0.90997	-1.27326	-1.17377
O	-2.19316	-1.64132	0.37497
H	-2.49637	-0.75333	0.09911
O	-0.33312	-2.81683	0.00286

RC3(M)-FAM

Si	-2.32003	0.18981	0.00805
O	-0.93369	1.05978	-0.35684
H	-0.95898	1.98877	-0.10952
O	-2.77808	0.80264	1.46041
H	-3.69497	0.68821	1.71875
O	-3.56156	0.46040	-1.03205
O	-1.91122	-1.37570	-0.08052
C	1.68135	-1.15377	0.06732
O	0.75853	-1.84394	0.44955
O	1.57089	0.07174	-0.42073
H	2.72963	-1.47499	0.08479
H	0.62916	0.38532	-0.42002
H	-3.61726	-0.12296	-1.79234
C	4.82626	0.89230	0.54483
H	5.77739	0.46698	0.87037
H	4.08185	0.72725	1.33639
H	-1.00841	-1.63943	0.18076
H	4.95862	1.97330	0.40755
O	4.47143	0.24403	-0.66055

H	3.60711	0.56751	-0.93659

TSM1-FAM

C	-1.84021	-0.81617	-0.28755
O	-1.27528	-1.03203	0.88560
O	-3.11474	-1.19973	-0.45569
H	-1.26518	-0.91211	-1.20936
H	-3.47383	-1.39676	0.42103
C	-2.94249	1.61668	0.05209
H	-3.56770	1.27918	0.88531
H	-2.66750	2.66161	0.20442
H	-3.49292	1.51025	-0.88512
O	-1.74155	0.85715	-0.03569
H	-1.33683	0.23385	0.89849
Si	1.88346	0.05242	-0.05846
O	3.43493	-0.07145	-0.58198
H	3.75255	-0.96395	-0.73347
O	1.50499	-1.41566	0.57232
H	0.56410	-1.51766	0.79756
O	1.74686	1.28847	1.03028
H	2.33178	1.26382	1.79000
O	0.85849	0.47289	-1.27727
H	0.17395	1.10777	-1.03822

TSM2-FAM

C	-2.08678	-0.40083	-0.63998
O	-1.21251	-1.45306	0.49073
O	-3.20263	-0.74777	-0.07508
H	-1.74866	-0.84908	-1.57653
H	-2.43773	-1.41438	0.60906
C	-2.13468	1.66375	0.51903
H	-1.73464	2.66129	0.34595
H	-3.22431	1.67328	0.52000
H	-1.76130	1.27168	1.46871
O	-1.64497	0.86502	-0.56919
H	-0.69622	-0.95310	1.15229
Si	1.73242	0.01938	-0.05120
O	3.34693	0.22447	0.11047
H	3.86906	-0.56796	0.24937
O	1.40211	-1.45972	-0.67015
H	0.56306	-1.86175	-0.40308
O	0.93808	0.04206	1.42958
H	1.15071	0.77430	2.01296
O	1.22628	1.28950	-0.95011
H	0.26851	1.33282	-1.06611

TSM3-FAM

C	-1.27659	1.87588	0.10717
H	-0.20887	2.10922	0.12571
H	-1.77913	2.52889	-0.61227
H	-1.68588	2.05770	1.11132
O	-1.44600	0.52317	-0.28343
H	-1.39263	-0.32027	0.62364
Si	1.88348	-0.14341	-0.05834
O	0.97557	-0.38582	1.30524
H	1.39847	-0.14013	2.13124
O	2.43679	1.40553	0.08350
H	3.19059	1.64295	-0.46097
O	3.21527	-1.10159	-0.18118
H	3.08880	-1.95172	-0.60853

O	0.92958	-0.44388	-1.34436
H	-0.00213	-0.17777	-1.26336
C	-3.06241	-0.11956	-0.06439
H	-3.50770	0.67926	0.54248
O	-2.21374	-1.05818	1.03918
H	-2.46904	-0.88768	1.95403
O	-3.51838	-0.69806	-0.99186

TSM4-FAM

Si	-2.01006	0.15234	-0.01810
O	-1.12553	-0.61252	1.18484
H	-1.59349	-1.30896	1.65403
O	-2.99704	-1.04344	-0.56381
H	-3.79128	-0.77570	-1.03040
O	-2.98592	1.34749	0.55340
O	-0.94388	0.82284	-1.03225
C	2.07368	-0.77411	-0.38552
O	1.25090	-0.70470	-1.28569
O	1.55342	-0.85210	1.08262
H	2.94299	-1.44437	-0.40475
H	0.56349	-0.77379	1.09861
H	-2.61501	2.23265	0.53389
C	4.13944	0.77281	0.05921
H	4.46467	0.76419	-0.98512
H	4.62759	-0.04753	0.60165
H	-0.12112	0.32295	-1.23928
H	4.42579	1.72271	0.51479
O	2.72646	0.66911	0.10934
H	2.13115	0.16938	1.08032

PC1(M)-FAM

C	2.13935	-0.11233	-0.86252
O	0.44413	2.72581	0.29331
O	2.58888	0.82383	-0.24495
H	1.93772	-0.11879	-1.93823
H	1.36607	2.45209	0.19295
C	2.01274	-1.40983	1.09766
H	1.74807	-2.43748	1.33888
H	3.05384	-1.20590	1.35200
H	1.35205	-0.71168	1.61568
O	1.82143	-1.29229	-0.32569
H	0.12129	2.24034	1.06482
Si	-1.47333	-0.18262	-0.08471
O	-3.11069	-0.06025	-0.04754
H	-3.60767	-0.61454	-0.65247
O	-0.67310	0.71316	-1.19060
H	-0.36460	1.58765	-0.87205
O	-0.96143	0.38055	1.39808
H	-1.56422	0.22392	2.12929
O	-1.12340	-1.76509	-0.35994
H	-0.21509	-1.93164	-0.63715

PC2(M)-FAM

C	1.55988	1.33699	-1.23371
H	0.54623	1.72827	-1.31556
H	2.28068	2.11618	-1.49570
H	1.67545	0.46314	-1.87915
O	1.72870	0.95463	0.14037
H	0.67013	-1.72827	-0.90361
Si	-1.74627	-0.00707	0.14271

O	-1.11400	-1.16945	-0.86282
H	-1.54573	-1.27340	-1.71484
O	-1.97037	1.29766	-0.84149
H	-2.60082	1.95725	-0.54326
O	-3.21178	-0.40158	0.76919
H	-3.21405	-0.84771	1.61901
O	-0.71249	0.19029	1.38013
H	0.20567	0.43406	1.18213
C	2.81548	0.21327	0.43150
H	3.49148	0.06471	-0.42355
O	1.62399	-1.85759	-1.03428
H	1.88663	-2.54286	-0.41485
O	3.00593	-0.21070	1.53701

PC3(M)-FAM

Si	-1.77409	-0.02169	-0.10357
O	-0.98526	1.31282	-0.71713
H	-1.16261	1.52803	-1.63580
O	-1.45607	-0.02144	1.50390
H	-0.66236	-0.51166	1.75322
O	-3.36317	0.21824	-0.42510
O	-1.30107	-1.41175	-0.83733
C	2.00763	-0.77902	0.62178
O	1.00432	-1.40931	0.88633
O	1.38125	1.94767	0.61986
H	2.63210	-0.29815	1.38626
H	0.56075	1.81123	0.11100
H	-3.93803	-0.54688	-0.35945
C	3.57176	0.20112	-0.82874
H	4.43114	-0.16162	-0.25752
H	3.31394	1.22302	-0.54357
H	-0.44160	-1.73989	-0.53522
H	3.79143	0.14081	-1.89279
O	2.43503	-0.65291	-0.62077
H	1.11597	2.45975	1.38748

RC1(T)-FAM

Si	0.60345	1.60998	-0.22324
O	-0.24626	1.94482	-1.57705
H	-1.12011	1.53253	-1.63785
O	-0.36345	0.71227	0.79131
O	1.95378	0.76095	-0.51308
O	1.02733	3.00155	0.52478
H	0.58596	3.79826	0.22421
Si	3.04673	-0.42766	-0.32345
Si	-0.57300	-0.93125	0.94549
O	4.50904	-0.08175	-0.96369
O	2.38112	-1.67219	-1.20220
H	2.92558	-2.45088	-1.33968
O	3.24729	-0.80536	1.25313
H	2.42849	-0.97113	1.74966
O	0.56896	-1.36342	2.07368
H	0.39018	-2.17139	2.56166
O	-2.05689	-1.25568	1.50106
H	-2.74793	-1.43271	0.82030
O	-0.33780	-1.67430	-0.49209
H	0.56243	-1.76658	-0.85061
H	5.14795	0.34493	-0.38870
C	-3.41443	-2.64572	-1.43375
H	-3.65598	-3.55589	-0.88260

H	-4.01404	-2.61937	-2.34974
H	-2.34761	-2.64623	-1.67940
O	-3.74076	-1.55025	-0.58323
H	-3.55931	-0.71813	-1.04303
C	-3.40632	1.83938	-0.04765
H	-4.38840	2.32643	-0.04542
O	-2.74879	2.07224	1.06139
O	-3.00225	1.17091	-0.98646
H	-1.89392	1.57478	1.06605

INTT

Si	0.42169	-1.42349	-0.57552
O	-0.70192	-2.36314	0.18474
H	-0.51882	-3.30374	0.24666
O	-0.29443	-0.01341	-0.91203
O	1.72325	-1.18487	0.39368
O	0.85405	-2.23989	-1.93191
H	1.57042	-1.87558	-2.45692
Si	2.94555	-0.09920	0.47973
Si	-0.40123	1.57715	-0.47892
O	4.37126	-0.80270	0.86458
O	2.48972	0.90934	1.71395
H	3.16147	1.50200	2.06017
O	3.12518	0.68410	-0.94706
H	2.44645	1.34791	-1.17850
O	0.88422	2.32781	-1.25246
H	0.65355	2.82226	-2.04279
O	-1.75561	2.24005	-1.06871
H	-2.56027	1.69727	-0.98766
O	-0.16245	1.76692	1.12360
H	0.72436	1.57952	1.47007
H	5.00317	-0.92851	0.15389
C	-2.58376	-0.01342	2.37178
H	-2.32864	-1.06688	2.52940
H	-1.77948	0.62144	2.74064
H	-3.51826	0.22163	2.89726
O	-2.69806	0.28352	0.98974
H	-2.49742	-1.86265	0.07554
C	-3.71555	-0.37753	0.32363
H	-4.66658	-0.29483	0.86727
O	-3.82448	0.30072	-0.90665
O	-3.46198	-1.72230	0.13597
H	-3.80826	-0.36585	-1.60113

RC2(T)-FAM

Si	1.00433	1.46989	0.61807
O	0.22891	1.86762	-0.79856
H	0.53734	1.30660	-1.52997
O	0.13423	0.36011	1.45509
O	2.45748	0.82585	0.23617
O	1.11297	2.83357	1.50095
H	1.02660	2.74716	2.45217
Si	2.76913	-0.46753	-0.75872
Si	-0.59169	-1.07914	1.18890
O	4.13201	-0.21989	-1.61816
O	1.52463	-0.51293	-1.84675
H	0.76211	-1.04157	-1.55204
O	2.89571	-1.82798	0.13761
H	2.21934	-1.99308	0.81381
O	0.50516	-2.19697	1.72850

H	0.21821	-3.11327	1.74405
O	-1.99286	-1.23883	2.00845
H	-2.60499	-0.50775	1.84534
O	-0.74977	-1.35801	-0.43221
H	-1.58081	-1.10335	-0.88471
H	4.95868	-0.17099	-1.13505
C	-3.19695	1.70446	-0.35578
O	-2.86907	0.96667	0.55519
O	-2.38391	2.36764	-1.13938
H	-4.24571	1.89978	-0.61286
H	-1.42973	2.18191	-0.92691
C	-4.09588	-1.68461	-1.16364
H	-5.06471	-1.51166	-1.64262
H	-3.86269	-2.75436	-1.17050
H	-4.13819	-1.33687	-0.13131
O	-3.06880	-0.92448	-1.80013
H	-2.99688	-1.18562	-2.72255

RC3(T)-FAM

Si	-0.25072	1.37378	-0.00986
O	0.37746	1.53529	1.50743
H	0.59080	2.42452	1.80139
O	0.18915	-0.06409	-0.57808
O	-1.88199	1.48628	-0.02500
O	0.39995	2.60183	-0.90755
H	-0.08261	2.87106	-1.69347
Si	-2.98703	0.26771	0.13966
Si	0.33659	-1.70144	-0.54016
O	-4.40821	1.01548	0.43951
O	-2.47057	-0.68334	1.41109
H	-2.39432	-0.24454	2.26330
O	-3.12089	-0.69660	-1.15709
H	-2.40504	-1.31979	-1.38260
O	-0.83932	-2.27849	-1.57527
H	-0.54350	-2.51006	-2.45908
O	1.79936	-2.16656	-1.05103
H	2.44682	-1.44973	-1.17570
O	-0.03479	-2.24132	0.95617
H	-0.90836	-1.95954	1.26750
H	-5.20785	0.53230	0.22110
C	2.86658	-1.33613	2.39337
H	1.99813	-1.99875	2.31617
H	3.74970	-1.87755	2.04772
H	3.02200	-1.05108	3.44242
O	2.72779	-0.19716	1.56057
H	1.90982	0.27053	1.77322
C	3.64437	0.99855	-0.74489
H	4.55028	0.78609	-0.17064
O	3.14799	0.23676	-1.54815
O	3.17698	2.20702	-0.46725
H	2.32127	2.35056	-0.91986

TST1-FAM

Si	0.63910	1.56697	0.26641
O	-0.15981	2.36442	-0.90695
H	-0.98291	1.95246	-1.22160
O	-0.36885	0.38285	0.86825
O	1.99451	0.83367	-0.23692
O	1.04709	2.61307	1.45678
H	0.59671	3.45992	1.44480

Si	3.15777	-0.27645	-0.46059
Si	-0.41784	-1.26432	0.62983
O	4.57820	0.34055	-0.98191
O	2.52896	-1.21387	-1.67937
H	3.10250	-1.88211	-2.06142
O	3.43201	-1.11810	0.91342
H	2.62923	-1.42093	1.36919
O	0.76440	-1.88029	1.62192
H	0.62272	-2.77979	1.92838
O	-1.85848	-1.83571	1.10872
H	-2.62285	-1.59649	0.54691
O	-0.16236	-1.62176	-0.94061
H	0.72367	-1.52533	-1.33032
H	5.20787	0.61024	-0.30983
C	-4.99260	-1.15370	-0.91260
H	-5.59374	-1.30040	-0.01012
H	-5.50311	-0.44189	-1.57560
H	-4.89619	-2.10994	-1.43427
O	-3.70516	-0.68663	-0.55703
H	-3.01359	-0.00550	-1.36527
C	-3.45249	1.10868	-0.17733
H	-4.49243	1.43225	-0.25533
O	-2.97073	1.26782	1.02463
O	-2.66924	1.11725	-1.23314
H	-2.01800	1.00461	1.05264

TST2-FAM

Si	0.42000	-1.39927	-0.54957
O	-0.70144	-2.40052	0.14945
H	-0.49981	-3.33984	0.15533
O	-0.34935	-0.01757	-0.87107
O	1.67159	-1.14326	0.47958
O	0.92342	-2.17529	-1.90393
H	1.60068	-1.74290	-2.43021
Si	2.91408	-0.07256	0.45552
Si	-0.45900	1.58292	-0.45445
O	4.34956	-0.77414	0.80387
O	2.53414	1.00281	1.65544
H	3.23167	1.59390	1.94914
O	3.01863	0.62683	-1.02322
H	2.35317	1.31039	-1.23896
O	0.81421	2.32077	-1.26321
H	0.56157	2.82744	-2.03914
O	-1.83177	2.22315	-1.00654
H	-2.63787	1.65924	-0.95186
O	-0.16939	1.77637	1.14176
H	0.74215	1.65767	1.44985
H	4.93626	-0.96689	0.06981
C	-2.41853	-0.32830	2.40826
H	-2.14145	-1.38633	2.34606
H	-1.59924	0.24166	2.84353
H	-3.32336	-0.21091	3.01520
O	-2.60927	0.21382	1.10836
H	-2.41231	-1.89987	-0.14958
C	-3.67814	-0.22117	0.40480
H	-4.55329	-0.44751	1.02824
O	-3.85174	0.39576	-0.75085
O	-3.35202	-1.64086	-0.28730
H	-3.50192	-0.81736	-1.10550

TST3-FAM

Si	-0.81609	-0.71359	1.40174
O	0.25455	-1.63992	0.52093
H	-0.08076	-1.77760	-0.38310
O	-0.39314	0.86775	1.31121
O	-2.30214	-0.92049	0.75816
O	-0.70124	-1.20756	2.94859
H	-0.82357	-0.54565	3.63182
Si	-2.78226	-0.77395	-0.82617
Si	-0.11925	1.95818	0.11729
O	-3.85718	-1.93517	-1.21635
O	-1.42672	-1.05843	-1.73068
H	-0.90696	-0.25699	-1.91856
O	-3.42770	0.70780	-1.06032
H	-2.96377	1.46896	-0.67637
O	-1.57099	2.71502	-0.11600
H	-1.55563	3.52008	-0.63992
O	1.02012	3.04802	0.53137
H	1.91163	2.67256	0.49560
O	0.23767	1.16654	-1.29465
H	1.16238	0.85512	-1.25964
H	-4.73508	-1.87349	-0.83596
C	3.44636	-0.08807	0.18372
O	2.65206	0.80421	-0.12788
O	2.88969	-1.42009	0.65931
H	4.32615	0.10284	0.81324
H	1.89000	-1.44752	0.61344
C	5.46481	-0.94460	-1.22975
H	5.97526	-1.26005	-0.31165
H	5.70786	-1.63843	-2.03580
H	5.79225	0.06056	-1.50804
O	4.05258	-0.94439	-1.06853
H	3.45919	-1.73943	-0.33034

TST4-FAM

Si	0.47786	-1.41949	-0.53653
O	-0.22124	-2.01900	0.83451
H	-0.17539	-2.97249	0.94015
O	-0.25425	-0.01143	-0.86327
O	2.09123	-1.20435	-0.35738
O	0.20798	-2.52922	-1.71497
H	0.80511	-2.53329	-2.46607
Si	3.04612	-0.03737	0.29957
Si	-0.45657	1.57009	-0.41737
O	4.48872	-0.74930	0.59092
O	2.29151	0.47097	1.70109
H	2.12584	-0.21142	2.35808
O	3.24361	1.26900	-0.63955
H	2.45911	1.79846	-0.87996
O	0.77878	2.42545	-1.15205
H	0.55163	2.84364	-1.98629
O	-1.84755	2.16236	-0.97918
H	-2.64508	1.59095	-0.99233
O	-0.23430	1.72659	1.19507
H	0.64776	1.48321	1.51850
H	5.25712	-0.17528	0.61614
C	-2.81986	0.13017	2.36775
H	-1.83286	0.20919	2.82111
H	-3.34379	1.08207	2.47642
H	-3.39342	-0.67973	2.83180

O	-2.61153	-0.11898	0.98145
H	-2.39492	-1.21274	0.51617
C	-3.85972	-0.34503	0.04573
H	-4.68469	-0.65705	0.70013
O	-3.97177	0.44596	-0.88053
O	-3.13977	-1.76209	-0.28802
H	-2.81401	-1.70934	-1.19895

PC1(T)-FAM

Si	-0.54441	1.41026	-0.51620
O	0.38921	2.64954	0.04151
H	0.00154	3.52789	0.04024
O	0.46206	0.15175	-0.68379
O	-1.72239	1.05050	0.57499
O	-1.21493	1.90270	-1.93017
H	-1.90052	1.33175	-2.29125
Si	-2.93764	-0.04802	0.52449
Si	0.52223	-1.49107	-0.52485
O	-4.37793	0.56752	0.99188
O	-2.47367	-1.20331	1.61406
H	-3.13725	-1.83926	1.89205
O	-3.08076	-0.62410	-1.00719
H	-2.38523	-1.24881	-1.29540
O	-0.76269	-2.05346	-1.45071
H	-0.53106	-2.70053	-2.12143
O	1.85337	-2.12923	-1.17763
H	2.73342	-1.75532	-0.97366
O	0.25457	-1.91135	1.03081
H	-0.64066	-1.76986	1.37538
H	-4.98090	0.86178	0.30629
C	2.43851	0.47427	2.22356
H	1.78908	1.26025	1.83467
H	1.89927	-0.14295	2.94024
H	3.32223	0.91975	2.68957
O	2.80928	-0.39098	1.14971
H	2.27249	2.50710	-0.23397
C	3.95011	-0.18437	0.51261
H	4.62475	0.55089	0.96920
O	4.21758	-0.80921	-0.49196
O	3.22795	2.35744	-0.29965
H	3.38525	2.09923	-1.21188

PC2(T)-FAM

Si	-0.63307	-0.80956	1.35879
O	0.44275	-1.70309	0.47871
H	0.19237	-1.76363	-0.45620
O	-0.24934	0.78758	1.31516
O	-2.13679	-1.00428	0.74684
O	-0.48030	-1.33698	2.89629
H	-0.72485	-0.72323	3.59169
Si	-2.63404	-0.80169	-0.82533
Si	-0.14380	2.02129	0.25023
O	-3.61912	-2.01562	-1.28979
O	-1.27157	-0.92177	-1.75201
H	-0.80824	-0.07937	-1.89910
O	-3.39717	0.63787	-0.95820
H	-2.99371	1.39187	-0.50031
O	-1.66305	2.66820	0.16929
H	-1.74079	3.51479	-0.27840
O	0.91429	3.16253	0.73952

H	1.84283	2.92654	0.62235
O	0.21067	1.43928	-1.26014
H	1.16719	1.30396	-1.37659
H	-4.48960	-2.05552	-0.88992
C	3.58682	0.37909	-0.54759
O	2.87316	1.35981	-0.46953
O	3.09241	-1.71225	1.34184
H	4.42347	0.18876	0.13567
H	2.16602	-1.78704	1.04746
C	4.29139	-1.65127	-1.51537
H	4.29322	-2.14224	-0.54026
H	3.89413	-2.31830	-2.27773
H	5.29327	-1.32159	-1.80214
O	3.39454	-0.52436	-1.48861
H	3.08434	-1.93775	2.27471

PC3(T)-FAM

Si	-0.57546	1.40325	-0.56874
O	0.37478	2.65241	-0.06130
H	-0.00164	3.53431	-0.11388
O	0.41807	0.12968	-0.69512
O	-1.74286	1.09579	0.55059
O	-1.24874	1.85021	-1.99349
H	-1.95462	1.28858	-2.32866
Si	-2.91646	-0.05049	0.54141
Si	0.54155	-1.50584	-0.55119
O	-4.30702	0.68727	0.98268
O	-2.48348	-1.25131	1.60867
H	-2.56119	-1.03909	2.54266
O	-3.05014	-0.72617	-0.93882
H	-2.35046	-1.34915	-1.22074
O	-0.71913	-2.07105	-1.50539
H	-0.60313	-2.95080	-1.87281
O	1.90582	-2.10306	-1.16971
H	2.77636	-1.74321	-0.90909
O	0.26275	-1.96287	0.99728
H	-0.65760	-1.88489	1.29210
H	-5.13038	0.22753	0.80645
C	2.35338	0.56357	2.21780
H	1.68132	1.30808	1.78808
H	1.83053	-0.03804	2.95995
H	3.21568	1.06246	2.66963
O	2.76407	-0.33389	1.18694
H	2.25799	2.49391	-0.30017
C	3.93330	-0.14898	0.59411
H	4.58697	0.60215	1.05537
O	4.24516	-0.80798	-0.37435
O	3.21617	2.34845	-0.32691
H	3.41172	2.08386	-1.22983

REFERENCES

(1) Venkateswarlu, P.; Gordy, W. Methyl Alcohol II. Molecular Structure. *J. Chem. Phys.* **1955**, *23*, 1200-1202.
(2) Herzberg, G. Electronic Spectra and Electronic Structure of Polyatomic Molecules, Van Nostrand, New York, 1966.
(3) Hellwege, K. H.; Hellwege, A. M. Landolt-Bornstein: Group II: Atomic and Molecular Physics Volume 7: Structure Data of Free Polyatomic Molecules. Springer-Verlag. Berlin, 1976.
(4) Hoy, A. R.; Bunker, P. R. A Precise Solution of the Rotation Beninding Schrodinger Equation for a Triatomic Molecule with Application to the Water Molecule. *J. Mol. Spect.* **1979**, *74*, 1-8.
(5) Gurvich, L. V.; Veyts, I. V.; Alcock, C. B. Thermodynamic Properties of Individual Substances, Hemisphere Pub. Co., New York, 1989.
(6) Glinnemann, J.; King Jr, H. E.; Schulz, H.; Hahn, T.; La Placa, S. J.; Dacol, F.; Crystal Structures of the Low-Temperature Quartz-Type Phases of SiO_2 and GeO_2 at Elevated Pressure. *Zeitschrift für Kristallographie-Crystalline Materials* **1992**, *198*, 177-212.
(7) Arnold, H. Die Struktur des Hochquarzes. *Zeitschrift für Kristallographie-Crystalline Materials* **1962**, *117*, 467-469.
(8) Kihara, K. An X-ray Study of the Temperature Dependence of the Quartz Structure. *Eur. J. Miner.* **1990**, 63-78.
(9) Viswanathan, K.; Brandt, K. The Crystal Structure of a Ternary (Ba, K, Na)-Feldspar and its Significance. *Am. Mineral.* **1980**, *65*, 472-476.
(10) Ribbe, P. H. A Refinement of the Crystal Structure of Sanidinized Orthoclase. *Acta Crystallogr.* **1963**, *16*, 426-427.
(11) Phillips, M. W.; Ribbe, P. H. The Structures of Monoclinic Potassium-Rich Feldspars. *Am. Mineral.* **1973**, *58*, 263-270.
(12) Gruner, J. W. The Crystal Structure of Kaolinite. *Zeitschrift für Kristallographie-Crystalline Materials* **1932**, *83*, 75-88.
(13) Bish, D. L. Rietveld Refinement of the Kaolinite Structure at 1.5 K. *Clays Clay Miner.* **1993**, *41*, 738-744.